

# Joint Centre for Mesoscale Meteorology, Reading, UK



## Parametrization of Momentum Transport by Convectively Generated Gravity Waves

**R. Kershaw**

**Internal Report No. 31**

**May 1994**

**Met Office** Joint Centre for Mesoscale Meteorology Department of Meteorology  
University of Reading PO Box 243 Reading RG6 6BB United Kingdom  
Tel: +44 (0)118 931 8425 Fax: +44 (0)118 931 8791  
[www.metoffice.com](http://www.metoffice.com)



# Parametrization of Momentum Transport by Convectively Generated Gravity Waves

By R. KERSHAW  
*Meteorological Office, UK*

Submitted to QJRMS 16 May 1994; revised 22 December 1994

## SUMMARY

A parametrization equation for momentum flux due to convectively generated gravity waves is derived and tested numerically. The wave momentum flux just above the convective layer is shown to depend directly on the shear and the intensity of convection, and inversely on the stability of the air above the convection. Simulations of ensembles of precipitating convective clouds are used to validate the parametrization and to estimate the efficiency of wave generation by convection in one particular convective regime: an idealised cold air outbreak with unidirectional shear.

## 1. INTRODUCTION

The association between gravity waves and convection has been known and exploited by glider pilots for many years. Bradbury (1990) gives an interesting review. Recent observations of the phenomenon using powered aircraft have been reported by Hauf (1993) and Kuettner et al (1987) above convective boundary layers in continental midlatitudes, and by Pfister et al (1993) above deep convection in the tropics. Convection waves have also been modelled numerically by Mason and Sykes (1982) (in 2-d, above a dry boundary layer), Clark et al (1986) (in 2-d, above shallow cumulus), Hauf and Clark (1989) (in 3-d, above shallow cumulus), and Fovell et al (1992) (in 2-d, above a deep squall line). An important result, supported by the observations and the modelling studies, is that the efficiency of wave generation depends on the strength of the vertical shear of the horizontal wind. (See for example the shear/no shear comparison in Clark et al.) In the presence of shear, waves which are quasi-stationary with respect to the convective eddies are generated, and these waves have phase lines which tilt upstream (in the frame of reference moving with the convection) with height (see especially Fovell et al).

These vertically propagating waves can transport momentum to higher levels in the atmosphere, and they may exert a significant acceleration (or deceleration) on the mean flow at levels where dissipation occurs, especially in the stratosphere and mesosphere. Therefore, it may be necessary to parametrize the effects of these waves in General Circulation Models (GCMs), just as it has been found necessary to parametrize the effects of orographically generated gravity waves (Palmer et al 1986). A full treatment of the problem requires a representation of the generation, propagation and dissipation of the waves. This paper is concerned mainly with the generation. There have been few attempts to parametrize this. Rind et al (1988) describe one such parametrization, but make no attempt to justify it. The purpose of this paper is to propose an alternative parametrization and to justify it theoretically and numerically.

## 2. THEORY

Consider the linear theory of monochromatic, vertically propagating, plane, sinusoidal, internal gravity waves in the  $x - z$  plane in a constant zonal flow  $U$  with constant static stability

$N^2$ . For simplicity we exclude sound waves and the effects of the earth's rotation. Following Holton (1992) p202, we obtain the dispersion relation

$$(Uk - \nu)^2 = \frac{k^2 N^2}{m^2 + k^2} \quad (1)$$

and the perturbation equation

$$k\hat{u} + m\hat{w} = 0 \quad (2)$$

where  $\nu$  is the frequency,  $k$  and  $m$  are the horizontal and vertical wavenumbers, and  $\hat{u}$  and  $\hat{w}$  are velocity amplitudes of the waves. The vertical momentum flux, averaged over several horizontal wavelengths is

$$\overline{\rho u w} = \frac{1}{2} \rho \hat{u} \hat{w} \quad (3)$$

where  $\rho$  is the density. Using equation 2 we obtain

$$\overline{\rho u w} = -\frac{1}{2} \rho \frac{m}{k} \hat{w}^2 \quad (4)$$

showing that the momentum flux depends on the slope of the waves  $m/k$  and the amplitude squared. If  $c_x = \nu/k$  is the horizontal phase speed

$$\hat{w} = (U - c_x) k \hat{h} \quad (5)$$

where  $\hat{h}$  is the displacement amplitude of the waves. Hence 4 becomes

$$\overline{\rho u w} = -\frac{1}{2} \rho m (U - c_x)^2 k \hat{h}^2. \quad (6)$$

Then, using the dispersion relation equation 1 to eliminate  $m$

$$\overline{\rho u w} = -\frac{1}{2} \rho \left( \frac{N^2}{(U - c_x)^2} - k^2 \right)^{\frac{1}{2}} (U - c_x)^2 k \hat{h}^2. \quad (7)$$

Following Mason and Sykes (1982), we can write this in terms of the Froude Number  $F = (U - c_x)k/N$

$$\overline{\rho u w} = -\frac{1}{2} \rho \sqrt{1 - F^2} F N^2 \hat{h}^2. \quad (8)$$

Equation 8 applies equally well to stationary waves generated by orography; in which case  $c_x = 0$ . It can be used to parametrize the near-surface momentum flux due to such waves. See, for example, Palmer et al (1986), where it is applied with the longwave approximation ( $F \ll 1$ ). To apply equation 8 to convection waves, we need to estimate the displacement ( $\hat{h}$ ) in terms of some measure of convective activity. We assume that some proportion  $\alpha$  of the convective kinetic energy  $\frac{1}{2} \rho_c \overline{w^2}_{max}$  can be converted to (potential plus kinetic) wave energy  $\frac{1}{2} \rho N^2 \hat{h}^2$  in the stable air above the convection. (Here  $\overline{w^2}$  is the vertical velocity variance over the horizontal domain and  $\overline{w^2}_{max}$  the maximum value of this quantity which occurs at mid level in the convection.  $\rho_c$  is the density at that same level.) Hence

$$\rho N^2 \hat{h}^2 = \alpha \rho_c \overline{w^2}_{max} \quad (9)$$

and

$$\overline{\rho u w} = -\frac{\alpha}{2} \rho_c \sqrt{1 - F^2} F \overline{w^2}_{max}. \quad (10)$$

Note that this analysis is only valid if  $F < 1$ . For small wavelengths ( $k > N/(U - c_x)$ ) the waves are evanescent and  $\overline{\rho u w}$  is zero. If  $F < 1$  we may approximate equation 10, to first order in  $F$ , by

$$\overline{\rho u w} = -\frac{\alpha}{2} \rho_c F \overline{w^2}_{max}. \quad (11)$$

So, writing  $U_{rel} = U - c_x$  and  $L_x = 2\pi/k$ , we obtain the following parametrization equation for the momentum flux due to convectively generated gravity waves

$$\overline{\rho u w} = -\pi \alpha \rho_c \frac{U_{rel} \overline{w^2}_{max}}{L_x N}. \quad (12)$$

A similar formula will hold for waves propagating in the  $y - z$  plane. The parameter  $\alpha$  can be thought of as the efficiency of wave generation by convection. It is likely to depend on the wind shear. In order to minimise that dependence and reflect the observed importance of wind shear, we make the following assumption: the waves are stationary with respect to the convective cells. This means that the horizontal phase speed of the waves is equal to the velocity in the middle of the convective layer, and so  $U_{rel}$  now represents the shear between that level and cloud top.

Equation 12 differs from the equation given in Rind et al (1988) (p335 equation 7) in several ways, most importantly: there is a direct linear dependence on the wind shear (Rind et al have none) and an inverse linear dependence on  $N$  (Rind et al have a direct linear dependence on  $N$ ). The observational and numerical evidence for the dependence on the wind shear has already been referred to. The damping effect of increased stability on wave activity above convection was reported by Mason and Sykes (1982). Equation 8 shows that, for small  $F$  and a given wave amplitude, the momentum flux is proportional to  $N$ . However, wave energy is proportional to  $N^2$ , so for a fixed excitation energy we obtain an inverse dependence of momentum flux (and also of wave amplitude  $\hat{h}$  or  $\hat{w}$ ) on  $N$ .

The next sections present a set of experiments which test equation 12 numerically, in one particular convective regime: an idealised cold air outbreak.

### 3. DESCRIPTION OF EXPERIMENTS

Whereas observational validation of equation 12 is difficult for a variety of reasons, requiring as it does accurate and simultaneous measurements in convective cloud and above it, numerical validation is perfectly feasible. A 3-d dynamical cloud model can be used to simulate ensembles of convective cloud for a range of controlled conditions, and the relevant quantities can be diagnosed. The simulations reported here tested the sensitivity of the momentum flux to variations in  $U_{rel}$ ,  $\overline{w^2}_{max}$  and  $N$ , and obtained a value for  $\alpha$ .

We used the Met Office cloud-resolving model described by Shutts and Gray (1994), which solves the anelastic equations for a 3-d rectangular Cartesian grid over a flat surface. The model predicts the time variation of the three velocity components  $u$ ,  $v$ , and  $w$ , pressure  $p$ , and thermodynamic variables  $T_l$  and  $q_t$ , which are conserved except when precipitation is formed:

$$T_l = T + \frac{gz}{c_p} - \frac{L_v q_l}{c_p} \quad (13)$$

$$q_t = q_v + q_l \quad (14)$$

where  $T$  is the absolute temperature,  $g$  the acceleration due to gravity,  $z$  the height above the surface,  $c_p$  the specific heat of dry air at constant pressure,  $L_v$  the latent heat of condensation of water,  $q_l$  the cloud water mixing ratio, and  $q_v$  the water vapour mixing ratio. The domain is a box with cyclic lateral boundary conditions and no flux of air through the top or bottom. There is a no slip condition at the surface and the surface fluxes of heat and moisture are constant and specified. The model has a positivity-preserving advection scheme and subgrid parametrization schemes for turbulence (1st order, stability dependent closure) and microphysics (Kessler-type warm rain). Although the model runs on an  $f$ -plane,  $f = 0$  in these runs: rotational effects

were not thought likely to be important at the horizontal scales considered here, and non-zero  $f$  complicates the model initialisation. (Recent work (Shutts and Gray 1994) casts some doubt on this assumption, so future experiments should be run to evaluate the effect of rotation on convection waves.)

For the majority of the experiments, we used a domain 50km square by 15km deep, and gridlengths of 1000m horizontally and 500m vertically, though we did re-run some experiments with a larger domain or smaller horizontal gridlength to test the robustness of the results. The resolution is comparable with that used in previous 3-d simulations of convection waves (eg Hauf and Clark 1989). We used horizontally uniform initial conditions, piecewise linear in height, and specified in terms of potential temperature, relative humidity, and the  $v$ -component of the wind (see Fig. 1). The other wind components  $u$  and  $w$  were initially zero, as was  $q_l$ , the cloud water. The control temperature profile was dry adiabatic to 1500m, conditionally unstable to 4km, and isothermal above the tropopause at 9km, giving convective cloud tops around 6km. The control value of  $N$  in the upper troposphere was  $.9 \cdot 10^{-2}$ , ranging up to twice that value in some runs. Convection was initiated by small ( $< .05\text{K}$ ) random temperature perturbations at each gridpoint of the lowest model level (height 250m), and maintained by the surface fluxes:  $100\text{W}/\text{m}^2$  sensible heat and  $400\text{W}/\text{m}^2$  latent heat. This surface moisture flux was doubled or tripled in some experiments to vary the intensity of the convection ( $\overline{w^2}_{max}$ ). These highly idealised initial conditions represent a mid-latitude cold air outbreak, with deep, precipitating shower clouds developing in varying unidirectional shear and with varying stability above the convection. Each experiment was run for at least two hours (some for six), and the statistical diagnostics such as  $\overline{w^2}$  and the momentum fluxes were averaged over each hour. Most experiments were run with a damping layer above 10km, but, as discussed later, this does not appear to have had any effect on the results below this level.

## 4. RESULTS

### (a) Control run

In the control run [180], precipitating convective clouds develop during the first hour, in the layer between 1 and 6km above the surface. The clouds (Fig. 2) appear to be randomly distributed, with a horizontal size of  $\sim 5\text{km}$ , elongated in the  $y$ -direction (along the shear). Below cloud base, the simulation actually has a cellular structure reminiscent of a convective boundary layer, which is organised by precipitation-driven downdraughts. The size of the cells ( $\sim 10\text{km}$ ) determines the cloud spacing. Above the cloud layer, vertical motions with a horizontal wavelength of 8 – 10km have been forced by the convection (Fig. 3). That these are vertically propagating gravity waves may not be immediately apparent, but inspection of vertical sections confirms that they are. Figure 4 shows patterns of alternating upward and downward motion tilting upstream (towards the left) with height. The corresponding anomalies in  $v$  (Fig. 5) are out of phase with  $w$ , implying negative momentum flux, and the anomalies in  $\theta$  (Fig. 6) are in quadrature, as expected. The waves penetrate into the model stratosphere, where they are artificially damped. (In the absence of a damping layer, the waves would be reflected at the model's rigid lid.) The waves are refracted upwards at the tropopause (9km), by the change in  $N^2$ , so that the vertical wavelength is reduced above that height. This is as predicted by linear theory (Gill 1982, p146). Apart from the discontinuity in  $N$  at the tropopause, the effects of which are discussed later, the lack of variation of  $N$  and  $V$  with height allows the waves to propagate into the stratosphere. The conditions for trapping or absorption at a critical layer are not satisfied (see for example Holton (1992) pp283-284).

The vertical profile of  $\overline{w^2}$  (Fig. 7), averaged over the horizontal domain, shows a peak in

Table 1: LIST OF EXPERIMENTS AND RESULTS FROM SECOND HOUR OF EACH RUN

experiment	shear m/s/6km	latent heat flux W/m <sup>2</sup>	stability (N) s <sup>-1</sup>	$\overline{w^2}_{max}$ m <sup>2</sup> /s <sup>2</sup>	$\overline{\rho v w}$ @ 8km N/m <sup>2</sup>
180	10	400	0.009	0.96	-0.016
181	20	400	0.009	0.82	-0.043
143	40	400	0.009	0.59	-0.070
183	10	800	0.009	1.68	-0.039
184	20	800	0.009	1.46	-0.091
185	30	800	0.009	1.42	-0.111
160	10	1200	0.009	2.48	-0.073
164	20	1200	0.009	2.16	-0.147
169	30	1200	0.009	1.96	-0.195
170	40	1200	0.009	2.06	-0.211
161	10	1200	0.012	2.52	-0.052
162	10	1200	0.015	2.48	-0.036
163	10	1200	0.018	2.48	-0.028

the convection layer at  $\sim 3\text{km}$  ( $\overline{w^2}_{max} = .96\text{m}^2/\text{s}^2$ ), and wave energy from 6 to 8km, decaying above. The corresponding profile of the momentum flux  $\overline{\rho v w}$  (Fig. 8) is negative and again shows a peak in the convection layer, with smaller, but significant, values in the gravity wave layer. The momentum flux in the direction perpendicular to the shear ( $\overline{\rho u w}$ ) is not significantly different from zero. It is important to realise that most of the momentum transport is due to the convection itself. The transport due to the waves peaks near cloud top, and it is this quantity which we seek to diagnose and parametrize. The convective fluxes themselves must not be allowed to contaminate the results. Because of this, we choose 8km, a level above cloud top but below the tropopause, at which to compare the momentum fluxes at the same time in other runs of the model to assess the effect of varying the shear, the intensity of convection, and the stability of the layer immediately above the convection. The results are presented in Table 1. Note that the magnitude of the wave momentum flux exceeds  $0.2\text{N}/\text{m}^2$  in the experiment with the largest shear and latent heat flux [170]. This is not negligible in comparison with orographic wave fluxes. Palmer et al (1986) reviewed the observational evidence (see their Table 1) and concluded that  $0.1\text{N}/\text{m}^2$  was a reasonable estimate of the average wave momentum flux observed by aircraft over orography, though in extreme events, such as downslope windstorms (Lilly 1978), the momentum flux can exceed  $1\text{N}/\text{m}^2$ .

(b) *Effect of shear*

Increasing the shear does increase the gravity wave momentum flux. This can be seen in Table 1 by comparing the results of sets of experiments in which only the shear is varied: [180,181,143], [183,184,185], and [160,164,169,170]. That this increase depends approximately linearly on the shear can be seen in Fig. 9. In this figure, the momentum flux is normalised by the convective intensity because convection is inhibited by increasing shear.

(c) *Effect of intensity of convection*

Increasing the intensity of convection also increases the gravity wave momentum flux. This can be seen in Table 1 by comparing the results of sets of experiments in which only the surface

flux of moisture is varied: [180,183,160], [181,184,164], [185,169], and [143,170]. Again, by normalising the momentum flux by the wind shear, the approximately linear dependence of the wave momentum flux on convective intensity can be seen (Fig. 10).

*(d) Effect of stability*

The results of one sequence of experiments [160,161,162,163] show that increasing the stability of the air immediately above cloud top does reduce the wave momentum flux. The inverse dependence on  $N$  can be seen in Fig. 11.

*(e) Estimate of efficiency factor  $\alpha$*

The results are summarised in Fig. 12, where  $\rho\overline{v\overline{w}}$  at 8km is plotted against what we might call the convective forcing  $-\pi\rho_c V_{rel} w_{max}^2 / L_y N$  in order to test the validity of equation 12. In constructing this graph we have taken:  $V_{rel}$  is  $v$  at 3km, and  $L_y = 10$ km. Thus we are assuming that the convective clouds move with the velocity in the middle of the convective layer and that the waves are stationary in that frame of reference. Inspection of animations from some simulations confirms that this is approximately true. The horizontal wavelength takes a spectrum of values in the experiments, and tends to be longer (10 – 14km) in the experiments with wind shear greater than the control. Nevertheless, constant  $L_y$  and zero (relative) phase speed are reasonable approximations, and, more importantly, they are the sort of approximations that would have to be made to apply the parametrization in a GCM.

Clearly, Fig. 12 shows that there is a strong linear relationship between the gravity wave momentum flux and the convective forcing. Within the range of these experiments, equation 12 is a reasonable approximation. The slope of the line of best fit in Fig. 12 gives  $\alpha = 0.18 \pm 0.05$ , which is a plausible estimate of the efficiency of wave generation.

However, the process of gravity wave generation by convection is, of course, a transient phenomenon. Although the convective activity has reached its maximum intensity in the second hour of each integration, the gravity wave activity has not. Indeed, in the third and subsequent hours the momentum fluxes at 8km are approximately doubled. This lag between the peak in convection and the peak in wave activity can be seen in Fig. 13. In the runs with the higher surface fluxes, the convective layer has deepened by the third hour, so that some of the momentum flux at 8km is due to the cloud transports themselves and not to the gravity waves. The efficiency factor  $\alpha$  can be calculated from equation 12 for each hour of the simulation and for all levels. Its magnitude at a particular level can be interpreted as the amount of wave energy which has reached that level, normalised by the convective energy. Figure 14 shows time series of  $\alpha$  for 8km and 10km from the control run [180] and Fig. 15 shows the vertical profile in the 4th hour. These figures suggest that 0.4 is a better estimate of  $\alpha$ . It is clear that the damping layer is having a marked effect on the waves above 10km, but most of the wave energy does reach that level. The apparent discontinuity in  $\alpha$  at 9km is caused by multiplying by the initial value of  $N$ , which is discontinuous at the tropopause.

*(f) Effect of damping layer*

With hindsight, the choice of a damping layer so close to the region of interest was unfortunate. However, the original purpose of the experiments was to study in-cloud fluxes. The gravity

wave results were serendipitous. In order to check whether the damping layer was corrupting the results, one of the experiments [164] was repeated with 10 extra levels, raising the top to 20km and the base of the damping layer to 15km [204]. Fig. 16 shows the vertical profiles of momentum flux for these two experiments, averaged over the second hour. There was no significant impact on the momentum fluxes below 10km of raising the damping layer. We conclude that the artificial damping has not had a damaging effect on the results. Fig. 17 shows the vertical profile of  $\alpha$  estimated from [204] for each of the six hours of the experiment. Again peak values of  $\alpha$  are about 0.4 at 10km decreasing to 0.3 around 12km.

### *(g) Effect of tropopause*

Because the vertical profile of momentum flux (Fig. 16) shows a marked decrease at the tropopause, we were initially concerned that wave energy might be trapped below the tropopause, leading to an unrealistic build up in a model with cyclic lateral boundary conditions. However, when we ran an experiment [231] with the same uniform gradient of  $\theta$  above 9km as below (ie without a stratosphere, see Fig. 1), but otherwise identical to [204], it became clear that the effect of the increase in stability at the tropopause is actually to reduce the wave momentum flux below the tropopause as well as above (Fig. 16). The wave energy above 10km (measured by  $\alpha$ ) is not much changed, on average, by the presence of the stratosphere (cf Figs. 18 and 17).

## 5. DISCUSSION

### *(a) Accuracy of efficiency estimate*

Whilst the experiments described above have confirmed that the momentum flux depends in the expected way on the intensity of convection, the shear and the stability, we cannot be as confident about the estimated value of  $\alpha$ . This is likely to depend on the organisation of the convection: for example, a squall line oriented perpendicularly to the shear might be expected to be more efficient at producing waves than a random field of cumulonimbus. (Certainly, 2-d simulations made with the model described above tend to give larger wave momentum fluxes than otherwise identical 3-d simulations.) Because convective organisation depends on the directional shear of the wind with height, as well as on the speed shear, cases with directional shear might give a different estimate of efficiency. The efficiency is also likely to depend on the scale of the convection, which can vary enormously from fair weather cumulus to tropical super-clusters. Further experiments are required to explore these areas.

Even within the narrow range of parameter space explored here, the estimates of  $\alpha$  are moderately sensitive to model resolution. Although doubling the domain size in a repeat of experiment [169] had no impact on the simulated convective intensity or the wave momentum flux, doubling the horizontal resolution (halving the gridlength to 500m) did. At 1000m resolution, the convective activity is not well resolved, much of it being subgridscale. At 500m resolution,  $\overline{w^2_{max}}$  is about 50% greater whereas  $\overline{\rho v w}$  is only 25% greater. Halving the gridlength again to 250m has little impact on  $\overline{w^2_{max}}$ . This suggests that the estimates of  $\alpha$  given above are likely to be about 15% too high.

### *(b) Wavelength selection*

What determines the wavelength of the generated waves? It is possible that the waves help to organise the flow, and so determine the scale of the convection, as suggested in Clark et al (1986),

Hauf and Clark (1989), and Sang (1993), all of which studied waves over shallow, boundary layer convection. However, inspection of animations of the model fields in our experiments suggests that the vertically propagating waves are generated near cloud top. The wavelength is presumably determined by the size and frequency of the convective cells; it appears to be well-defined from the initial stages of generation, making it unlikely that resonance is involved in the scale selection. The cloud separation does not seem to be the determining factor either. In the experiments with stronger shear than the control the clouds have a tendency to form streets, elongating in the direction of the shear. This explains the longer wavelengths in these experiments.

FDR (1992) studied stratospheric waves excited in 2-d simulations of a severe squall line and also found a sensitivity to the shear near cloud top. In these simulations, high frequency waves propagate away from the squall and their period (and hence their slope) is determined by the periodicity of the convective cells. Presumably, the horizontal wavelength is also determined by the length scale of the convective cells. In the presence of shear, quasi-stationary waves (relative to the storm) develop, having longer horizontal wavelengths than the high frequency waves. It is not clear what determines the horizontal wavelength, but in this case resonance seems unlikely, simply because the waves are confined to a uniform stratosphere.

### (c) Drag and acceleration

The momentum budget for the cloud model reduces to

$$\frac{\partial(\rho\bar{v})}{\partial t} = -\frac{\partial(\rho\bar{v}\bar{w})}{\partial z} - \frac{\partial(\rho\bar{v}_s\bar{w}_s)}{\partial z}. \quad (15)$$

There are no lateral flux terms because of the cyclic boundary conditions. The subscript  $s$  labels subgridscale quantities. Thus the vertical derivative of the momentum fluxes (resolved and subgrid) determines the acceleration.

Parametrization of the momentum flux near cloud top is only part of the problem. What really matters is where that momentum is transferred to, and where it is taken from. The propagation and dissipation of the waves are beyond the scope of this paper, but they can probably be dealt with in the same way as orographic gravity waves, save that their non-zero phase speed must be taken into account. However, convection waves will produce a momentum source near cloud top (orographic waves just exert a torque on the solid earth). It is necessary to account for this momentum source in any parametrization of convectively generated gravity waves in a GCM, otherwise a spurious sink of momentum will be introduced.

Figure 8 shows that the convection is decelerating the flow in the upper half of the cloud layer and accelerating the flow below. In the absence of waves, the momentum flux would be zero at cloud top. Therefore, the waves are accelerating the flow near cloud top and decelerating it above. In this convective regime (with downgradient transport by the convection) this means that the waves are opposing the tendency of the clouds to exert a drag near cloud top, and effectively spreading that drag over a deeper layer above. This is confirmed by comparing the experiments with differing stabilities above the convection. Calculation of fluxes partitioned between cloudy and clear air enables the flux due to the waves to be isolated from the convective fluxes. Figure 19 confirms that the momentum source due to the waves is confined to a relatively narrow ( $\sim 2\text{km}$ ) region near cloud top. There is little effect below that region. In particular the value of the surface stress is unaffected by the waves. This stress will largely be determined by the low level flow, which is dominated by precipitation-driven downdraughts.

*(d) Effect of vertical variations of wind speed*

Another caveat needs to be added to this analysis. We have assumed that vertical variations of  $v$  above the wave generation region do not affect the momentum flux near cloud top. In some circumstances that may not be true. In particular, if trapping or resonance occurs, or if there is a critical line too close to cloud top, the wave momentum flux may be significantly different from that predicted by the simplified theory presented here. This should be tested in further numerical experiments.

## 6. CONCLUSIONS

A parametrization equation for momentum flux due to convectively generated gravity waves has been derived and tested numerically. Simulations of ensembles of precipitating convective clouds were used to validate the parametrization and to estimate the efficiency of wave generation by convection, in idealised conditions representing a mid-latitude cold air outbreak, with deep, precipitating shower clouds developing in varying unidirectional shear and with varying stability above the convection. The simulations confirm that the momentum flux has a direct, linear dependence on the wind shear near cloud top and the intensity of convection, and an inverse linear dependence on the stability above cloud top. They also show that the momentum flux due to convectively generated waves is potentially significant when compared with that due to orographic waves. The parametrization, equation 12, should be validated in a wider range of convective regimes (including squall lines and more complex vertical variations of  $v$ ), by further numerical experiments. Some of these should be at higher resolution, to try to determine  $\alpha$ , the efficiency factor, more accurately, and others should be designed to clarify the process of wavelength selection (using single clouds and spectral analysis techniques). We plan to run such experiments.

We also plan to test the parametrization in a GCM. In doing so we will need to relate the convective intensity  $\overline{w^2}_{max}$  to the output of the model's convective parametrization scheme. Estimation of the wavelength of the waves is likely to prove one of the main uncertainties in applying the parametrization.

## REFERENCES

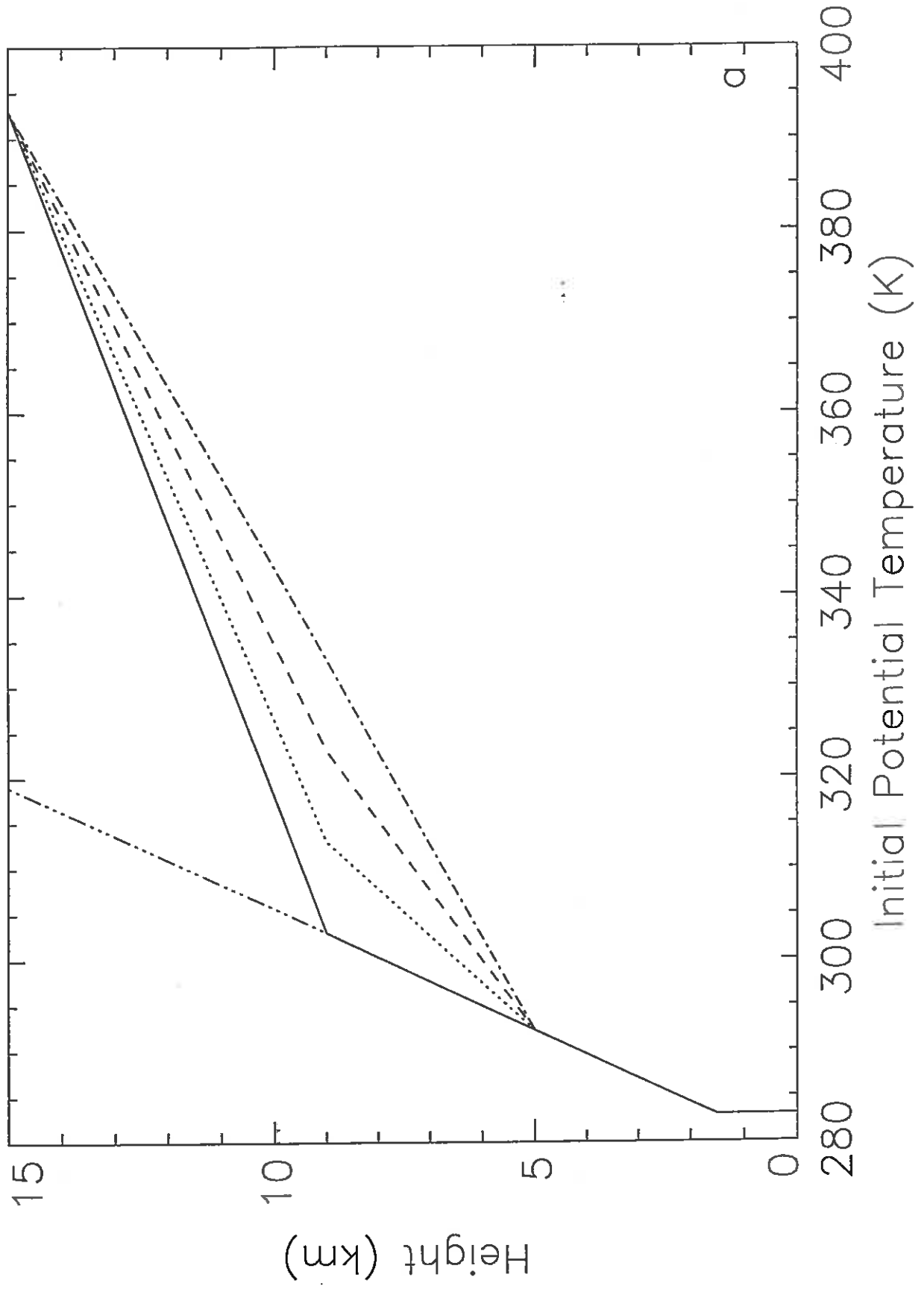
- Bradbury, T. A. M. (1990) Links between convection and waves. *Meteorol. Mag.*, **119**, 112–120
- Clark, T. L., Hauf, T. and Kuettner, J. P. (1986) Convectively forced internal gravity waves: Results from two-dimensional numerical experiments. *Q. J. R. Meteorol. Soc.*, **112**, 899–925
- Fovell, R., Durran, D. and Holton, J. R. (1992) Numerical simulations of convectively generated stratospheric gravity waves. *J. Atmos. Sci.*, **49**, 1427–1442
- Gill, A.E. (1982) *Atmosphere-ocean dynamics*. Academic Press. International Geophysics Series. Vol. 30
- Hauf, T. (1993) Aircraft observations of convection waves— a case study. *Mon. Weather Rev.*, **121**, 3282–3290
- Hauf, T. and Clark, T. L. (1989) Three-dimensional numerical experiments on convectively forced internal gravity waves. *Q. J. R. Meteorol. Soc.*, **115**, 309–333
- Holton, J. R. (1992) *An introduction to dynamic meteorology*. Third edition. Academic Press. International Geophysics Series. Vol. 48
- Kuettner, J. P., Hildebrand, P. A. and Clark, T. L. (1987) Convection waves: Observations of gravity wave systems over convectively active boundary layers. *Q. J. R. Meteorol. Soc.*, **113**, 445–467
- Mason, P. J., and Sykes, R. I. (1982) A two-dimensional numerical study of horizontal roll vortices in an inversion capped planetary boundary layer. *Q. J. R. Meteorol. Soc.*, **108**, 801–823
- Palmer, T. N., Shutts, G. J. and Swinbank, R. (1986) Alleviation of a systematic westerly bias in general circulation and numerical weather prediction models through an orographic gravity wave drag parametrization. *Q. J. R. Meteorol. Soc.*, **112**, 1001–1039
- Pfister, L., Scott, S. and Loewenstein, M. (1993) Mesoscale disturbances in the tropical stratosphere excited by convection: Observations and effects on the stratospheric momentum budget. *J. Atmos. Sci.*, **50**, 1058–1075
- Rind, D., Suozzo, R., Balachandran, N. K., Lacis, A. and Russell, G. (1988) The GISS global climate-middle atmosphere model. Part I: Model structure and climatology. *J. Atmos. Sci.*, **45**, 329–370
- Sang, J. G. (1993) On the dynamics of convection waves. *Q. J. R. Meteorol. Soc.*, **119**, 715–732
- Shutts, G. J. and Gray, M. E. B. (1994) A numerical modelling study of the geostrophic adjustment process following deep convection. *Q. J. R. Meteorol. Soc.*, (to appear in July, part B)

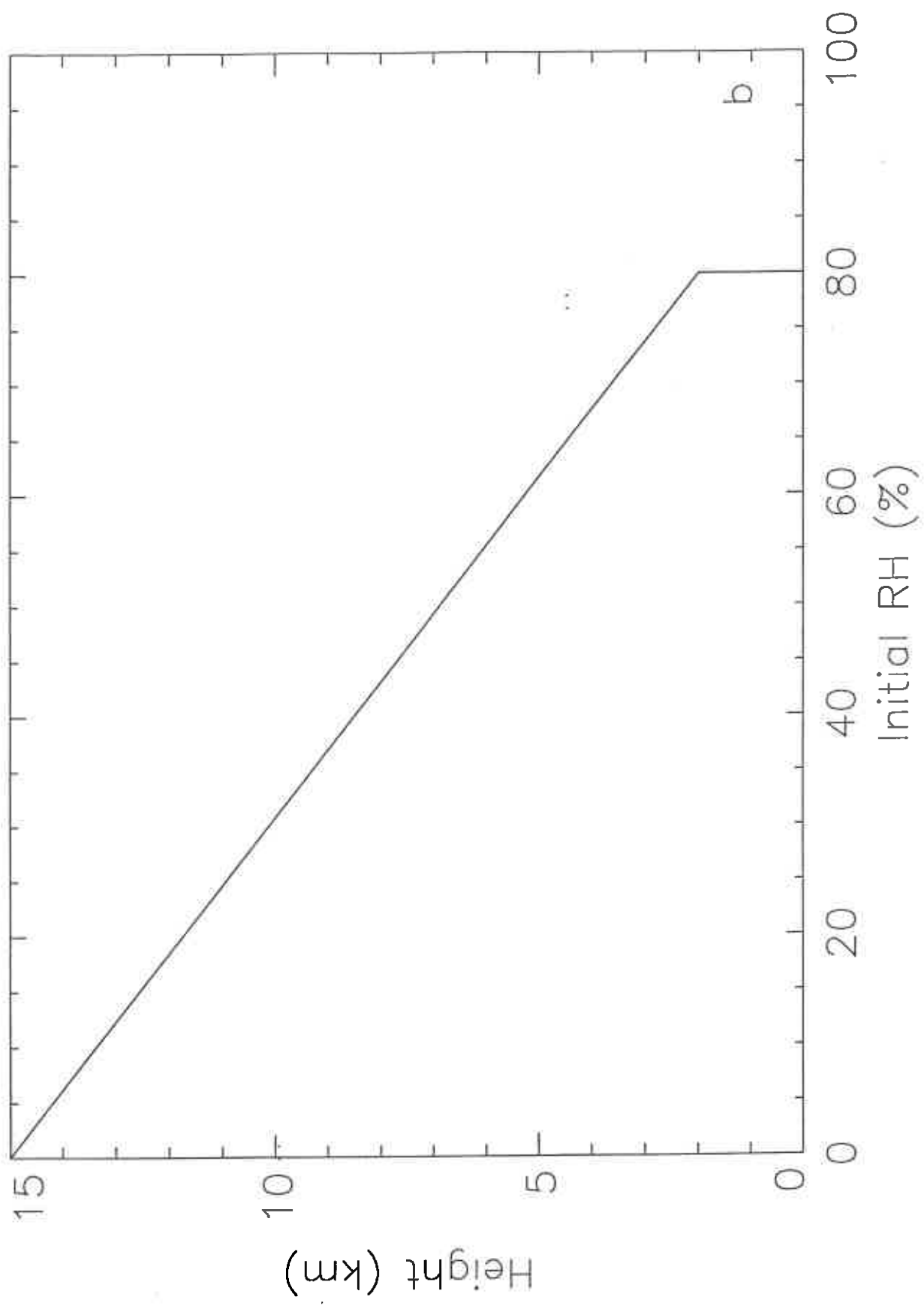
## List of Figures

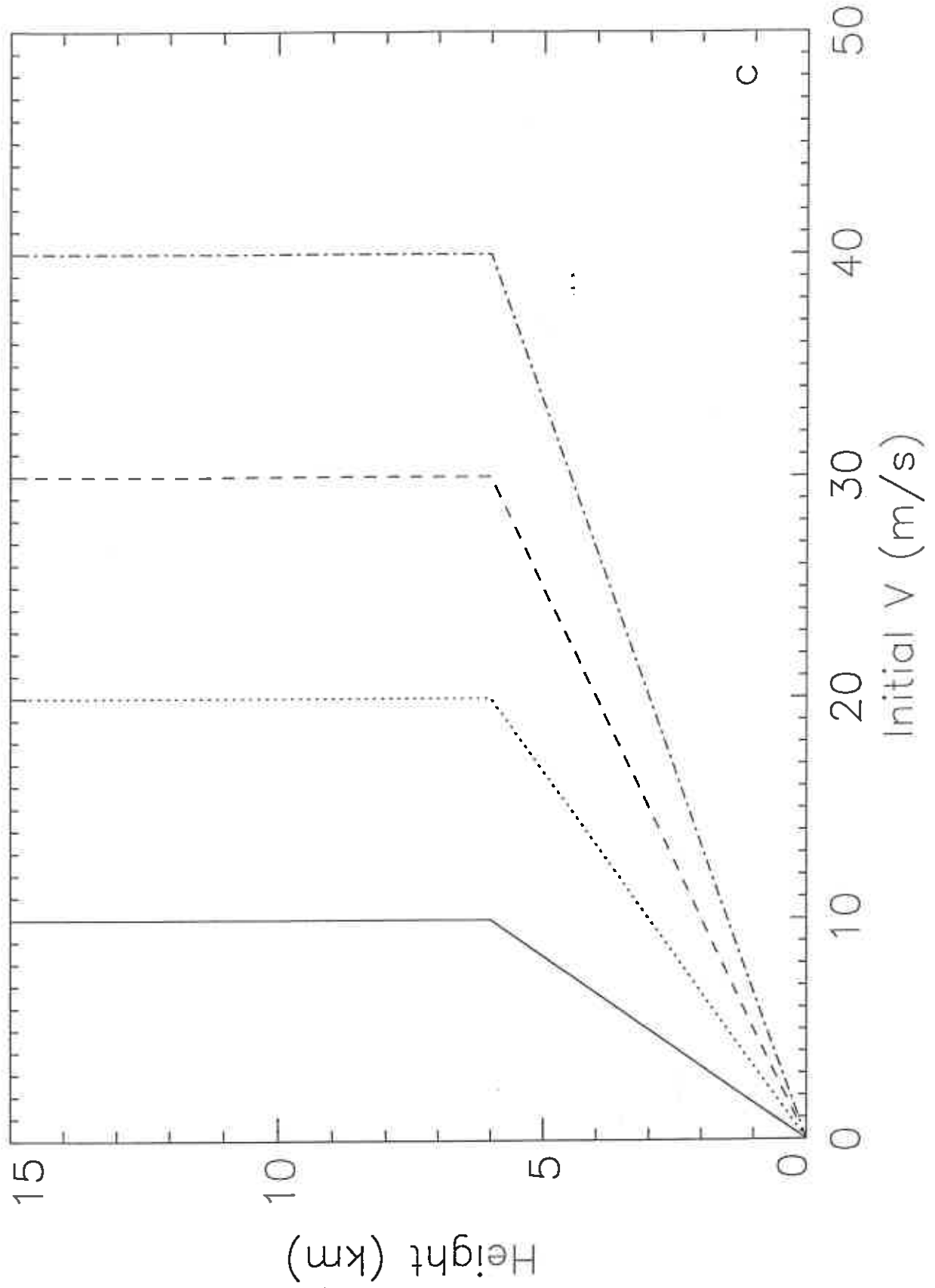
- 1 Initial profiles of (a) potential temperature, (b) relative humidity, and (c)  $v$ -component of the horizontal wind. Solid lines: control [180]. Broken lines: other experiments. . . . .
- 2 Horizontal section through control simulation [180] showing cloud water content at 4km, after 2 hours. Contour interval: 0.2 g/kg, first contour at 0.1 g/kg. . . .
- 3 Horizontal section through control simulation [180] showing vertical velocity at 8km, after 2 hours. Contour interval: 0.2m/s, dashed contours negative. . . . .
- 4 Vertical ( $y - z$ ) section through control simulation [180] showing vertical velocity at  $x = 25$ km, after 2 hours. Contour interval: 0.2m/s, dashed contours negative. The horizontal wind blows from left to right. . . . .
- 5 Vertical ( $y - z$ ) section through control simulation [180] showing perturbation of  $v$  component of velocity at  $x = 25$ km, after 2 hours. Contour interval: 0.3m/s, dashed contours negative. . . . .
- 6 Vertical ( $y - z$ ) section through control simulation [180] showing perturbation of potential temperature at  $x = 25$ km, after 2 hours. Contour interval: 0.2K, dashed contours negative. . . . .
- 7 Vertical profile of  $\overline{w^2}$  ( $\text{m}^2/\text{s}^2$ ) averaged over second hour of control simulation [180].
- 8 Vertical profile of  $\overline{\rho v w}$  ( $\text{N}/\text{m}^2$ ) averaged over second hour of control simulation [180]. . . . .
- 9 Scatter plot of magnitude of momentum flux at 8km, normalised by  $\overline{w^2}_{max}$ , plotted against wind shear. . . . .
- 10 Scatter plot of magnitude of momentum flux at 8km, normalised by wind shear, plotted against  $\overline{w^2}_{max}$ . . . . .
- 11 Scatter plot of magnitude of momentum flux at 8km plotted against  $N^{-1}$ . . . . .
- 12 Scatter plot of  $\overline{\rho v w}$  ( $\text{N}/\text{m}^2$ ) at 8km plotted against  $-\pi \rho_c V_{rel} \overline{w^2}_{max} / L_y N$  estimated from the second hour of the numerical experiments. The straight line is the least squares fit to the data. . . . .
- 13 Time series of  $\overline{w^2}_{max}$  (solid) and  $\overline{w^2}$  at 8km (dashed) averaged over each hour of control run [180]. . . . .
- 14 Time series of  $\alpha$  at 8km (solid) and 10km (dashed) from [180]. . . . .
- 15 Vertical profile of  $\alpha$  above 8km from 4th hour of [180]. . . . .
- 16 Vertical profile of momentum flux from 2nd hour of [164] (solid), [204] (dashed) and [231] (dash-dotted). . . . .

- 17 Vertical profile of  $\alpha$  above 8km from second and subsequent hours of [204]. . . . .
- 18 Vertical profile of  $\alpha$  above 8km from second and subsequent hours of [231]. . . . .
- 19 Vertical profile of partitioned momentum fluxes from the 2nd hour of a repeat of the control simulation with additional diagnostics (solid line: convective flux; stars: wave flux). . . . .

Figure 1: Initial profiles of (a) potential temperature, (b) relative humidity, and (c)  $v$ -component of the horizontal wind. Solid lines: control [180]. Broken lines: other experiments.







c

Figure 2: Horizontal section through control simulation [180] showing cloud water content at 4km, after 2 hours. Contour interval: 0.2 g/kg, first contour at 0.1 g/kg.

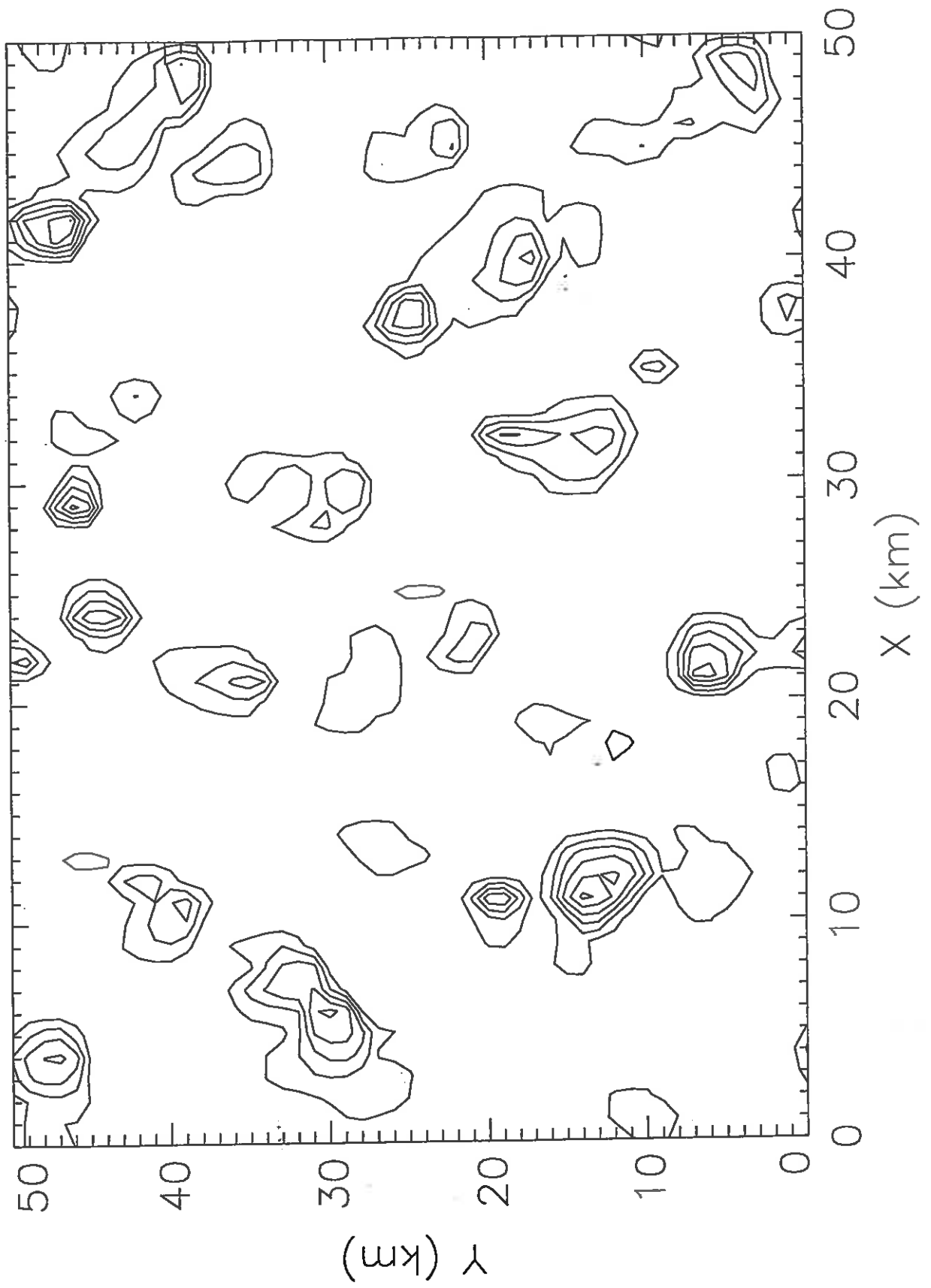
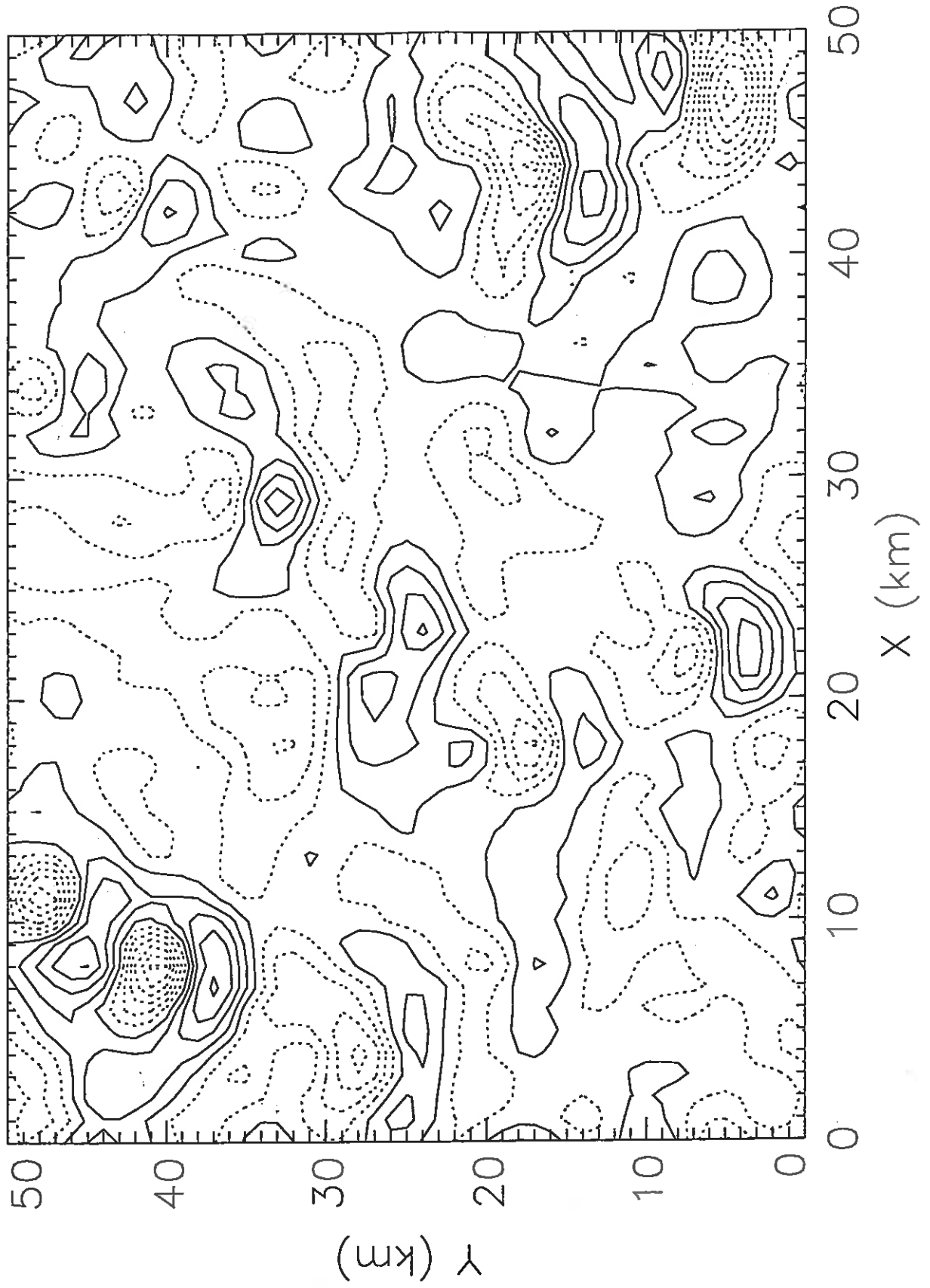


Figure 3: Horizontal section through control simulation [180] showing vertical velocity at 8km, after 2 hours. Contour interval: 0.2m/s, dashed contours negative.



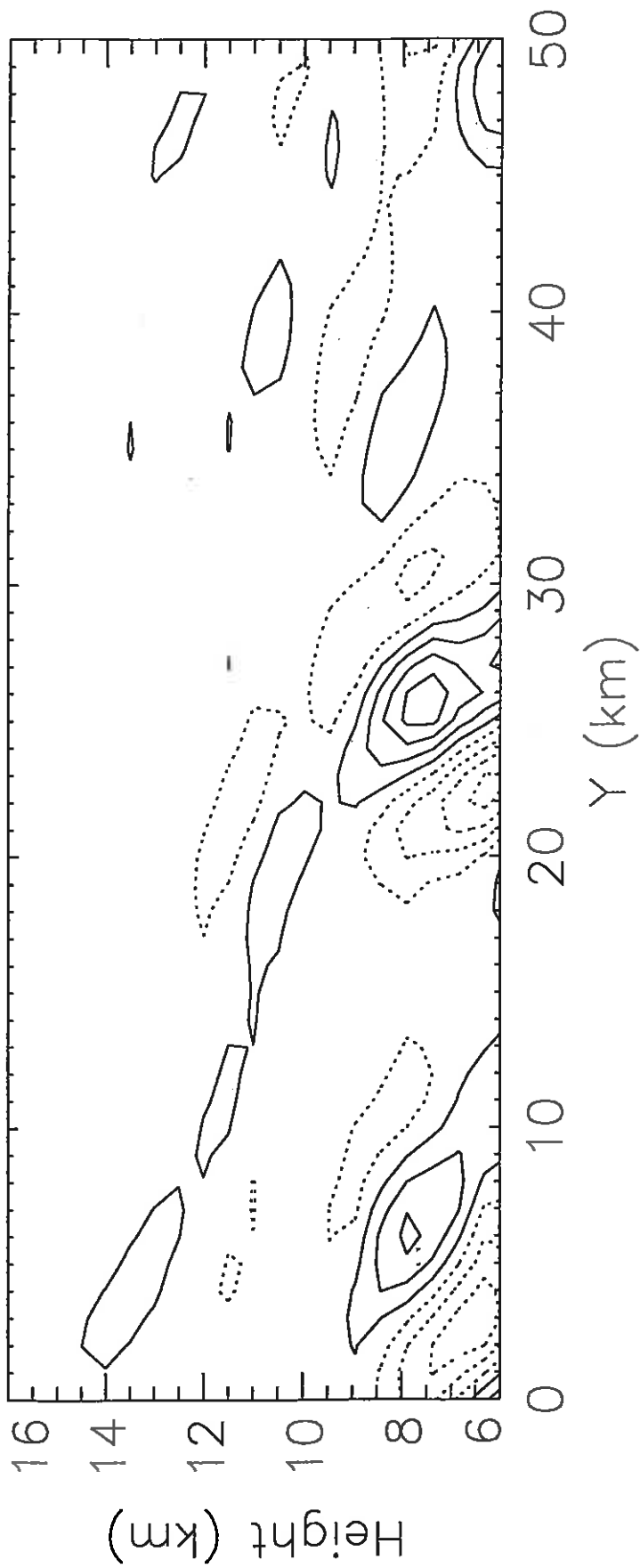


Figure 4: Vertical ( $y-z$ ) section through control simulation [180] showing vertical velocity at  $x = 25\text{km}$ , after 2 hours. Contour interval:  $0.2\text{m/s}$ , dashed contours negative. The horizontal wind blows from left to right.

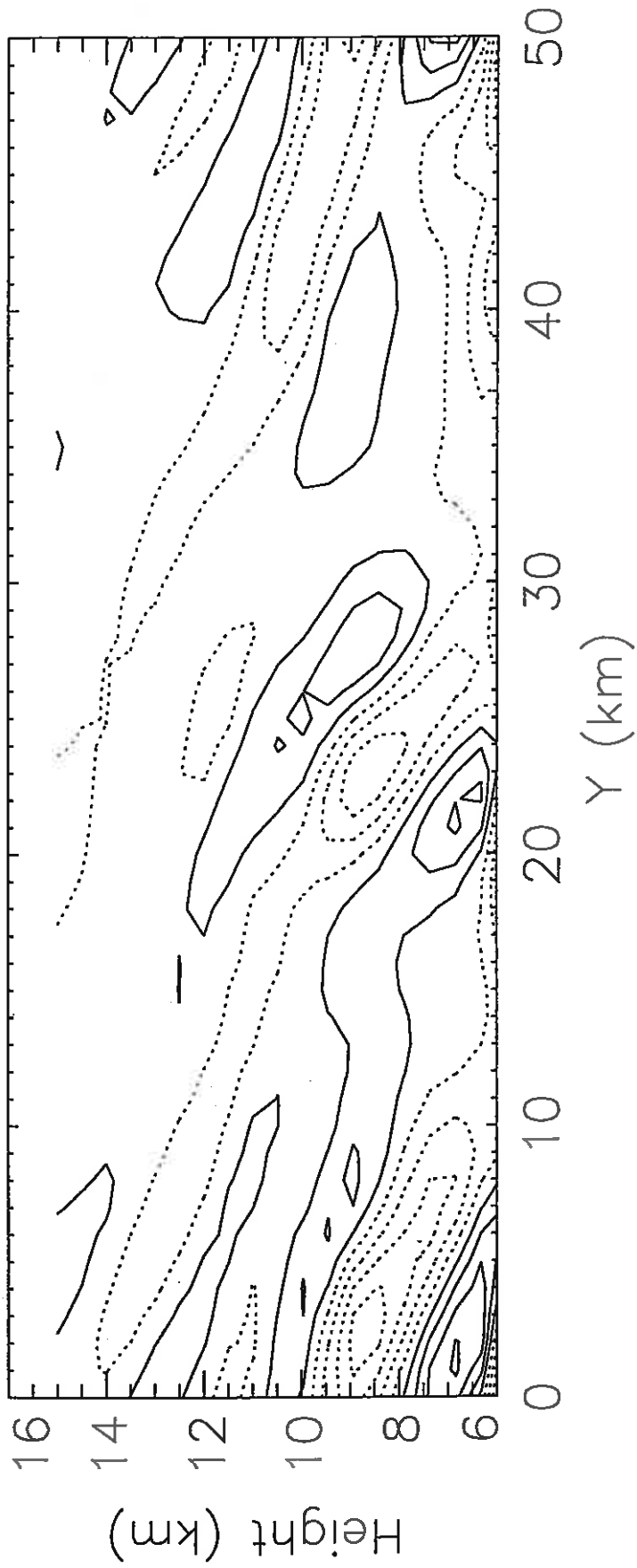


Figure 5: Vertical ( $y - z$ ) section through control simulation [180] showing perturbation of  $v$  component of velocity at  $x = 25\text{km}$ , after 2 hours. Contour interval:  $0.3\text{m/s}$ , dashed contours negative.

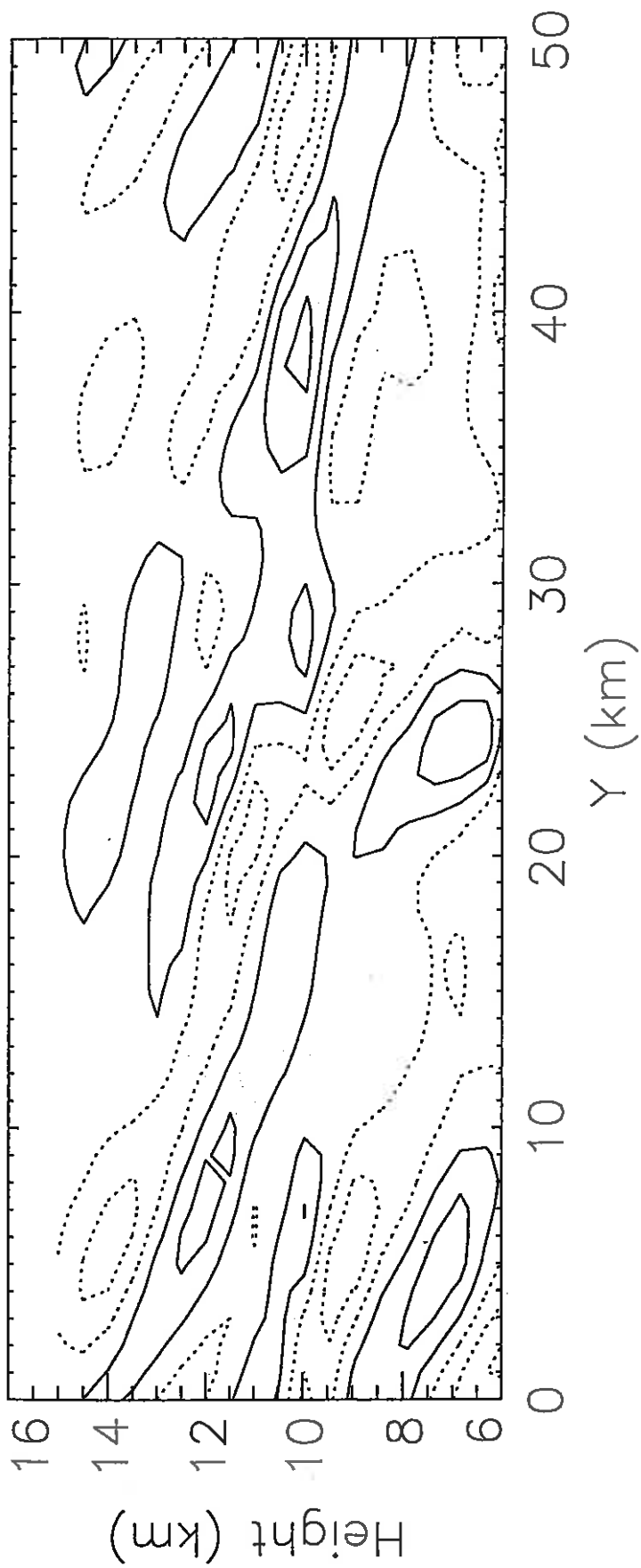


Figure 6: Vertical ( $y - z$ ) section through control simulation [180] showing perturbation of potential temperature at  $x = 25\text{km}$ , after 2 hours. Contour interval:  $0.2\text{K}$ , dashed contours negative.

Figure 7: Vertical profile of  $\overline{w^2}$  ( $\text{m}^2/\text{s}^2$ ) averaged over second hour of control simulation [180].

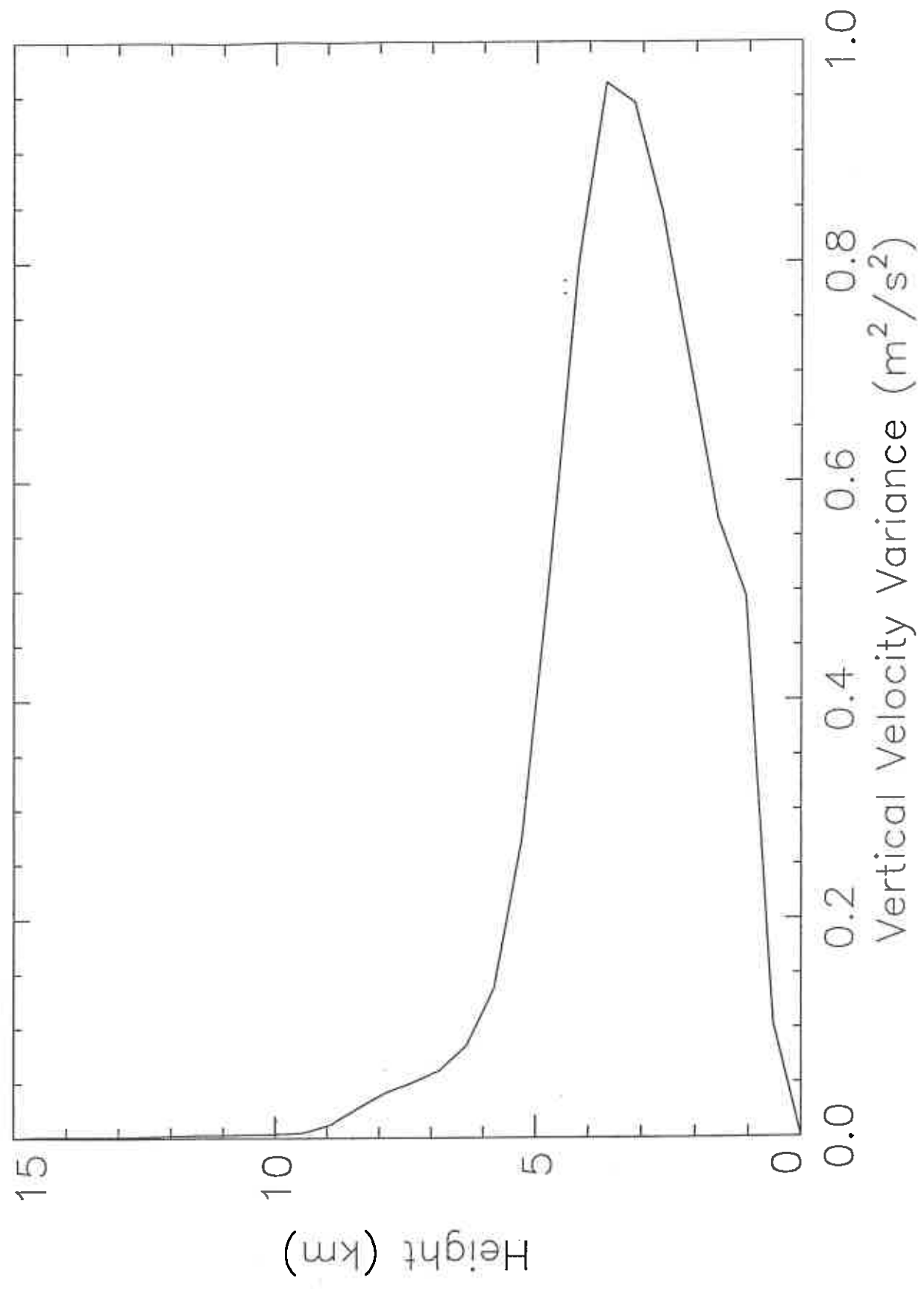


Figure 8: Vertical profile of  $\rho \overline{v w}$  ( $\text{N}/\text{m}^2$ ) averaged over second hour of control simulation [180].

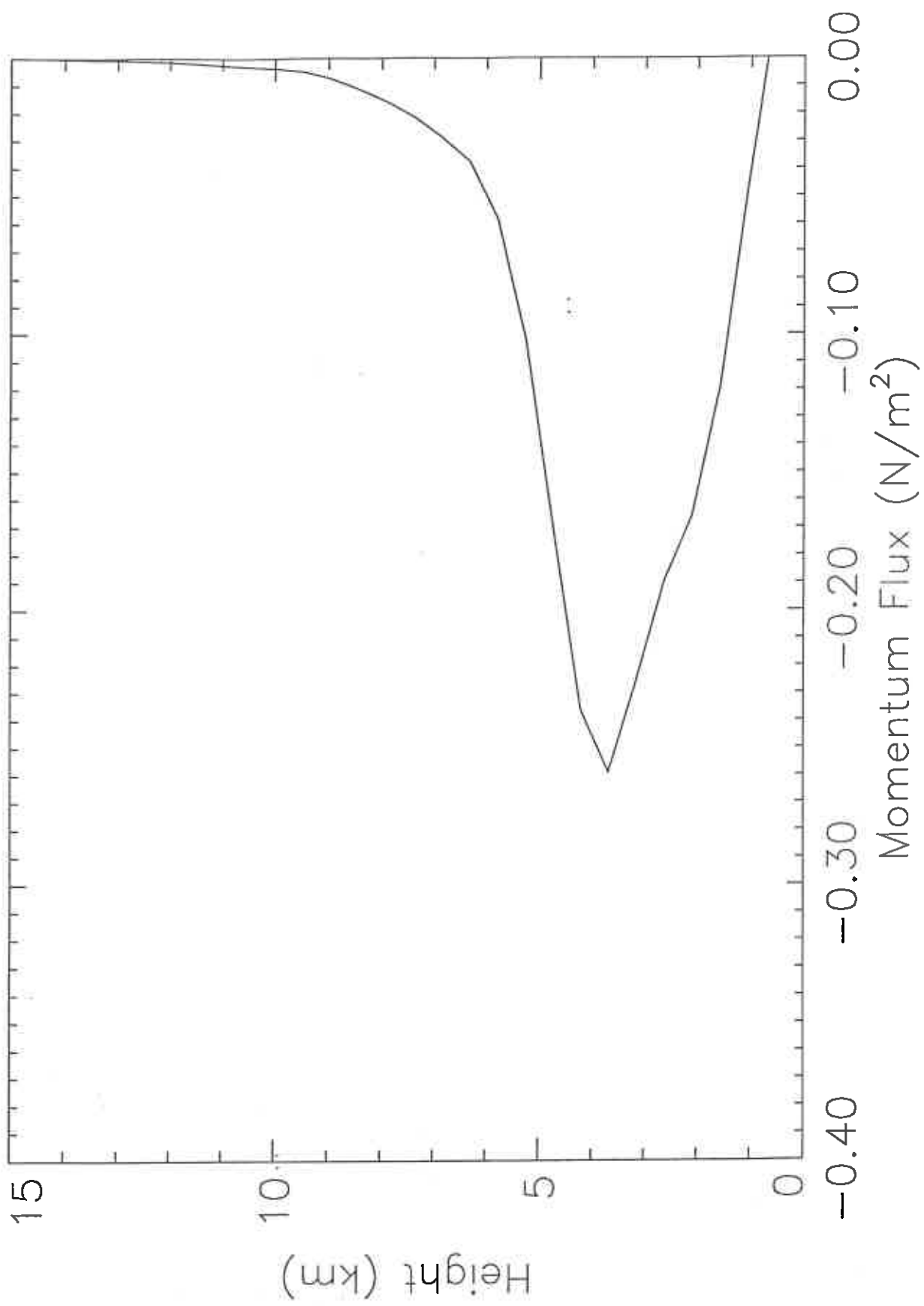


Figure 9: Scatter plot of magnitude of momentum flux at 8km, normalised by  $\overline{w^2}_{msr}$ , plotted against wind shear.

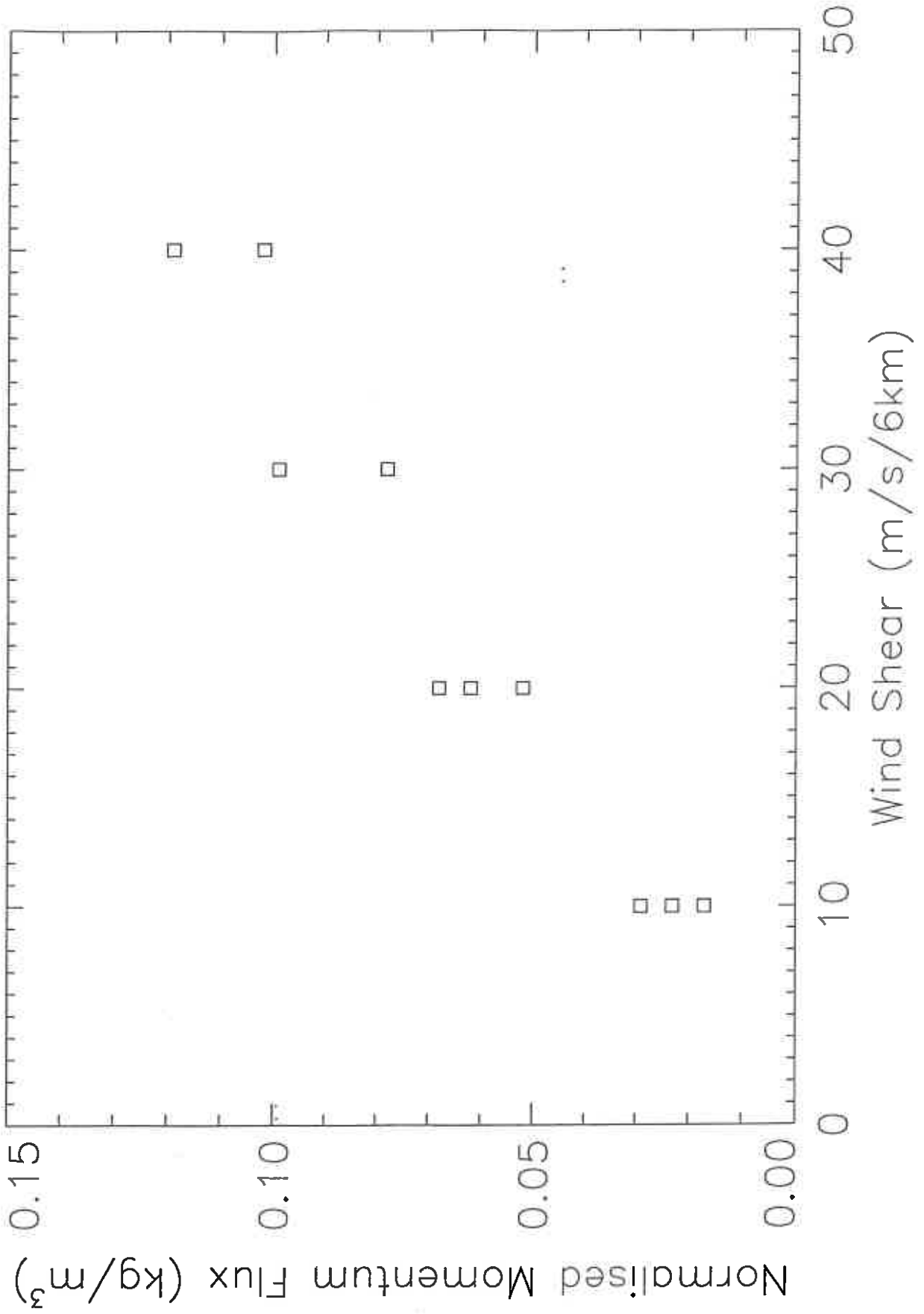


Figure 10: Scatter plot of magnitude of momentum flux at 8km, normalised by wind shear, plotted against  $w_{mar}^2$ .

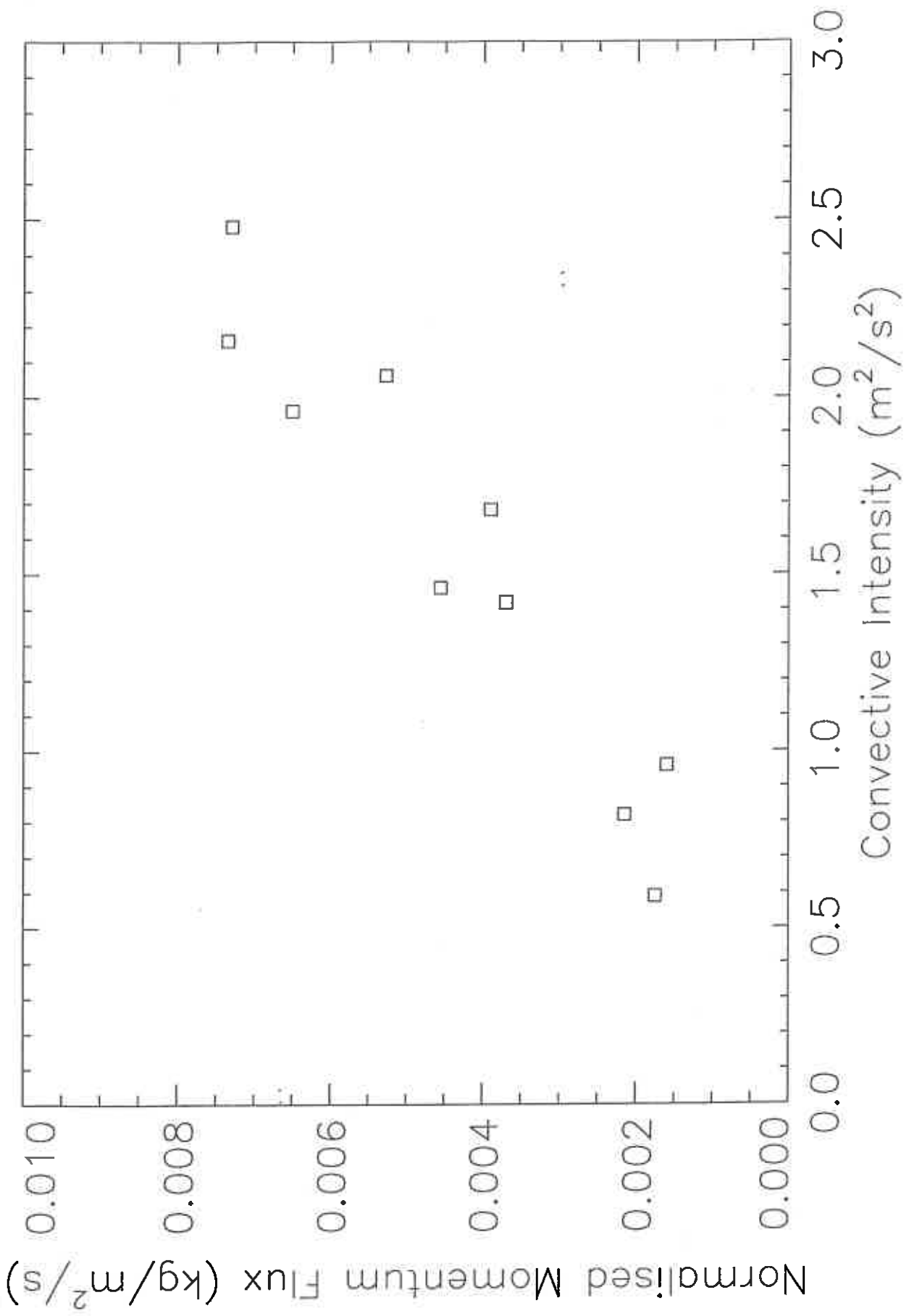


Figure 11: Scatter plot of magnitude of momentum flux at 8km plotted against  $N^{-1}$ .

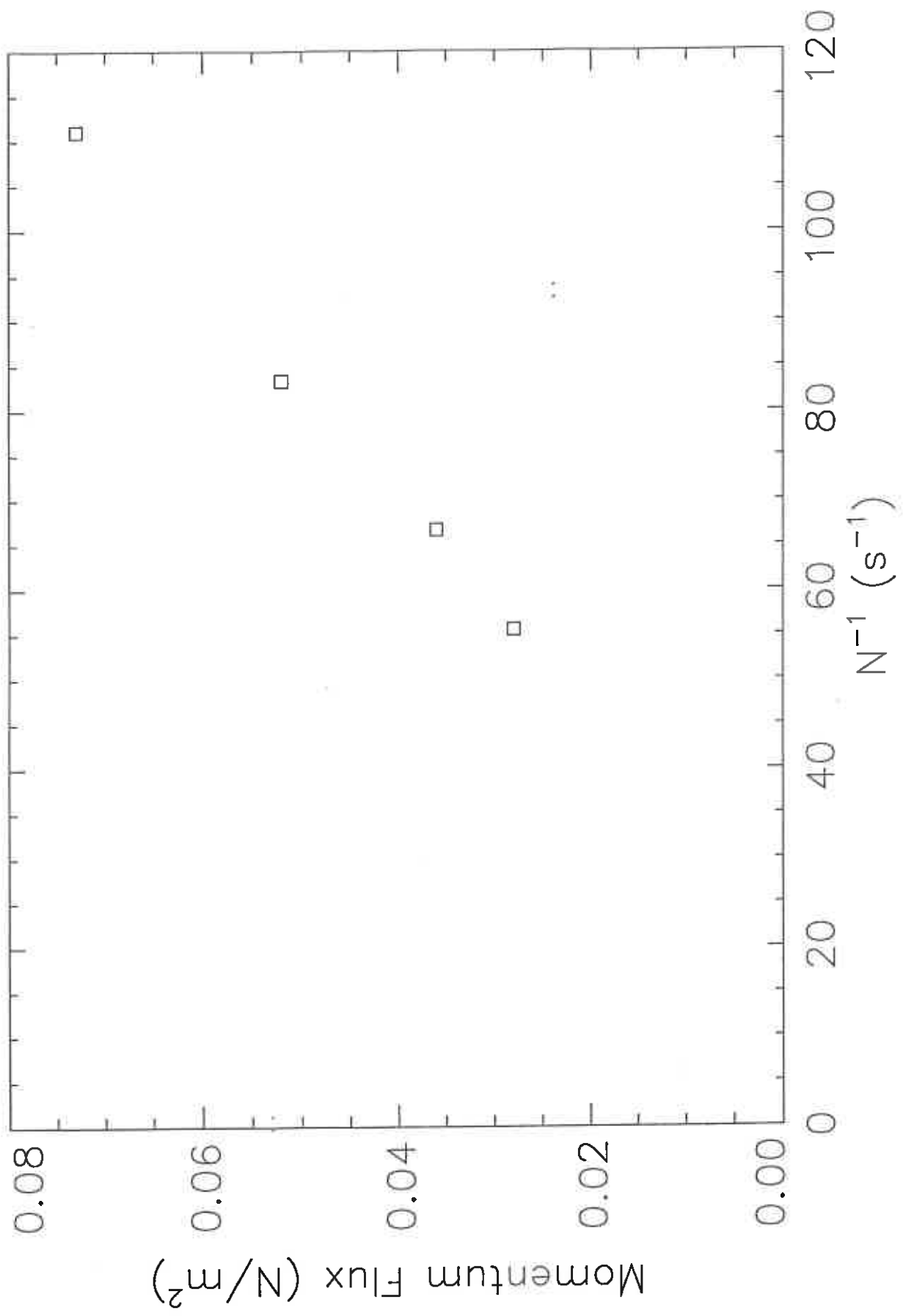


Figure 12: Scatter plot of  $\overline{\rho v w}$  ( $N/m^2$ ) at 8km plotted against  $-\pi \rho_c V_{ret} \overline{w^2}_{max} / L_y N$  estimated from the second hour of the numerical experiments. The straight line is the least squares fit to the data.

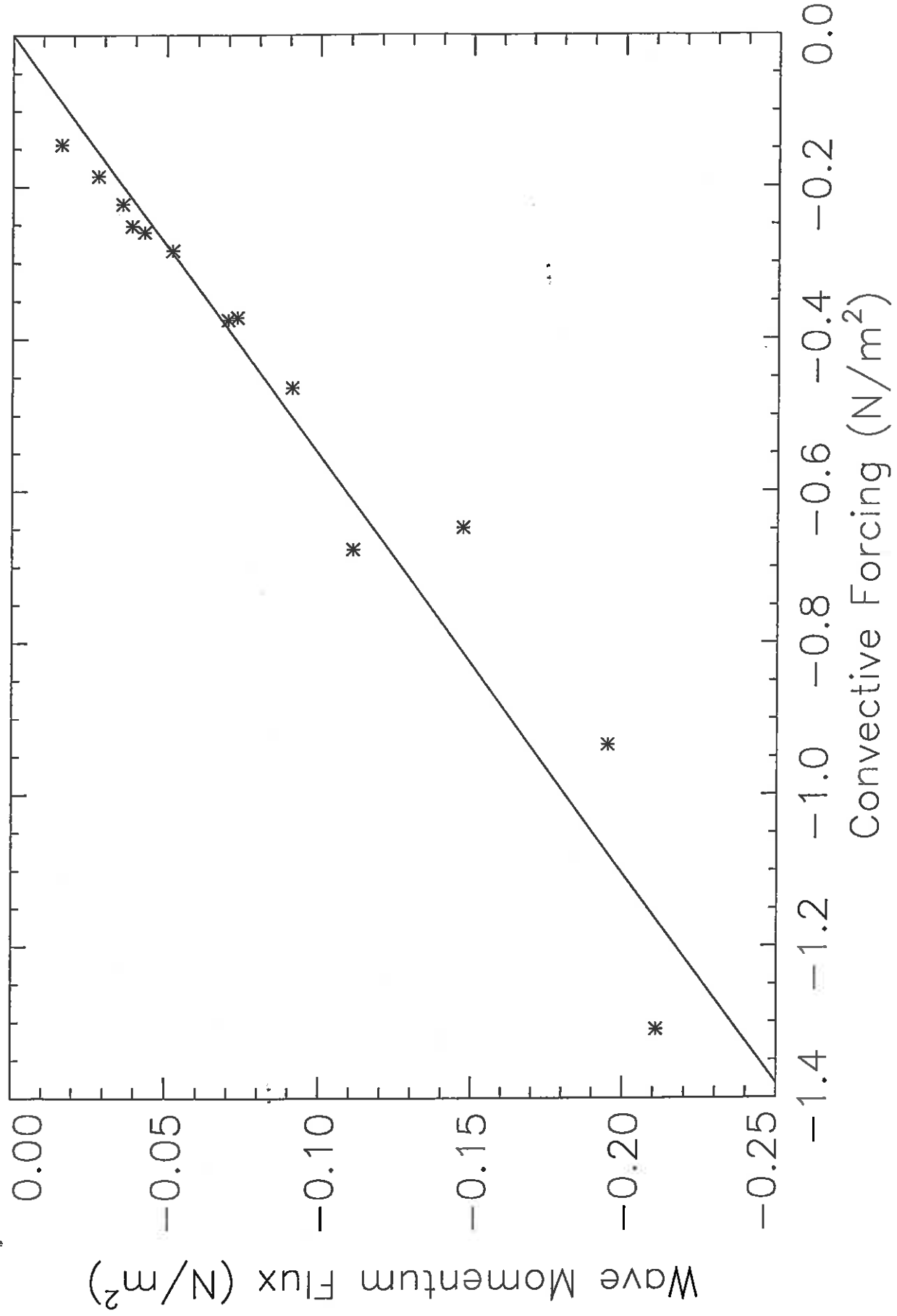


Figure 13: Time series of  $\overline{w^2}_{max}$  (solid) and  $\overline{w^2}$  at 8km (dashed) averaged over each hour of control run [180].

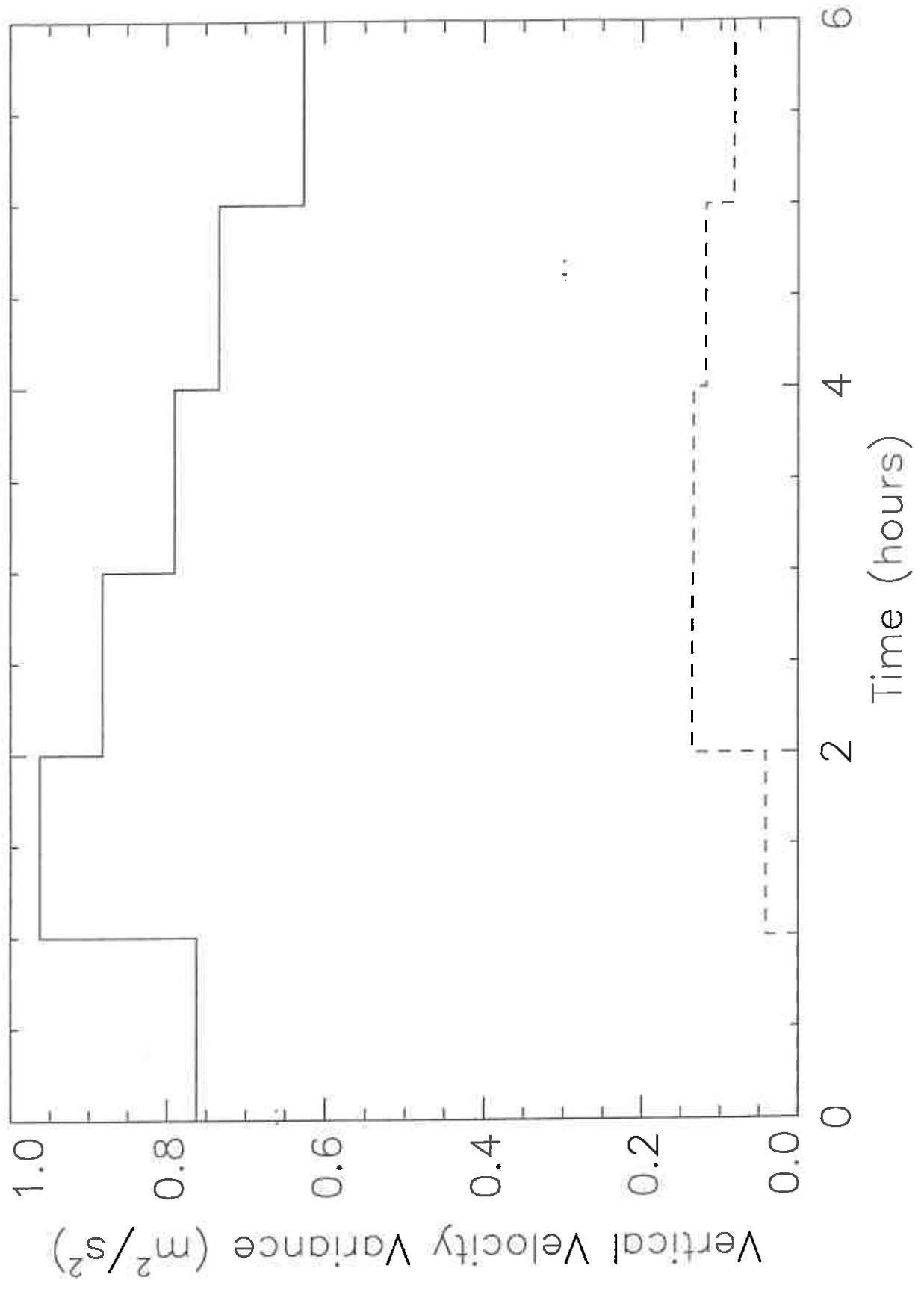


Figure 14: Time series of  $\alpha$  at 8km (solid) and 10km (dashed) from [180].

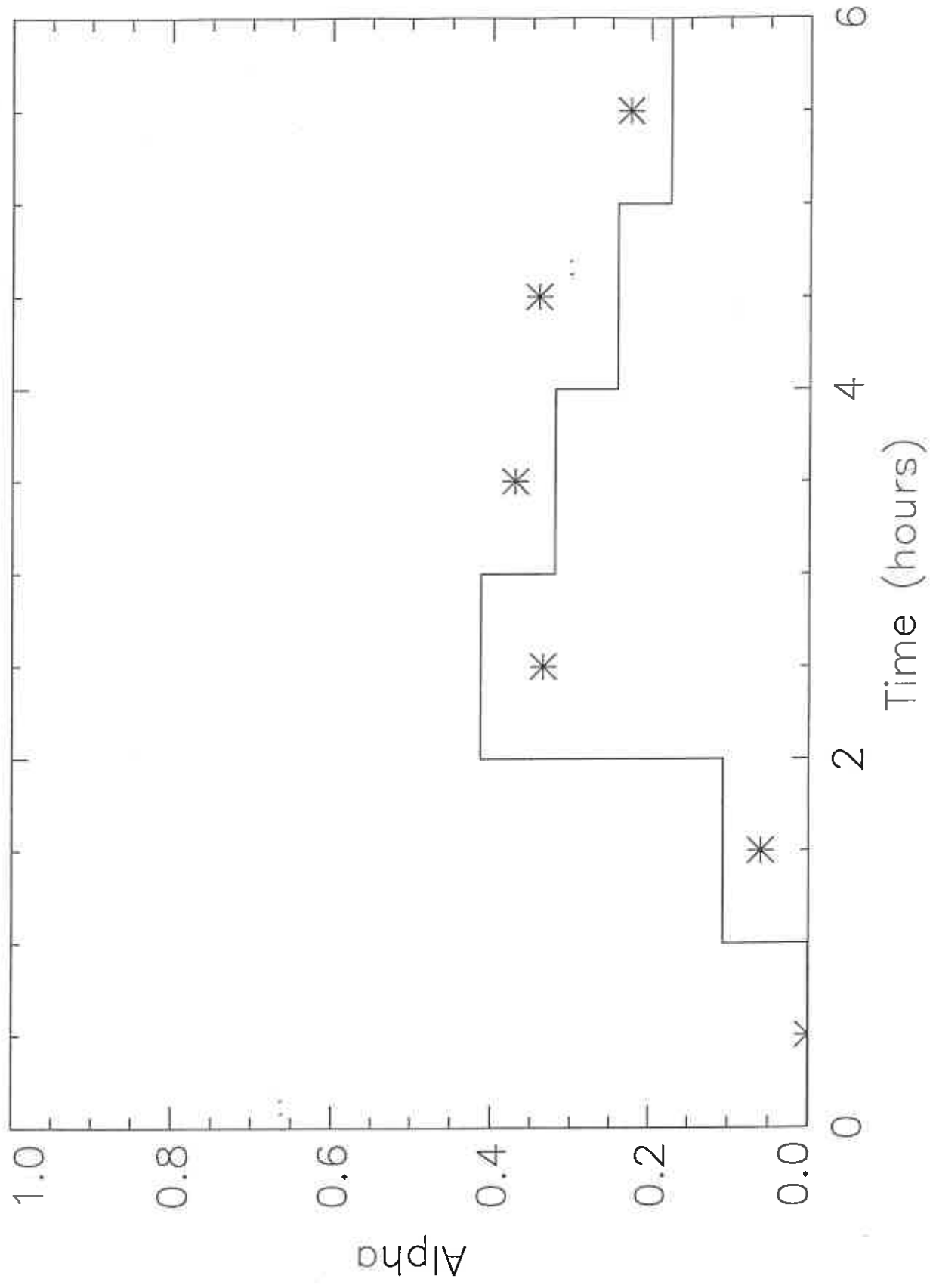


Figure 15: Vertical profile of  $\alpha$  above 8km from 4th hour of [180].

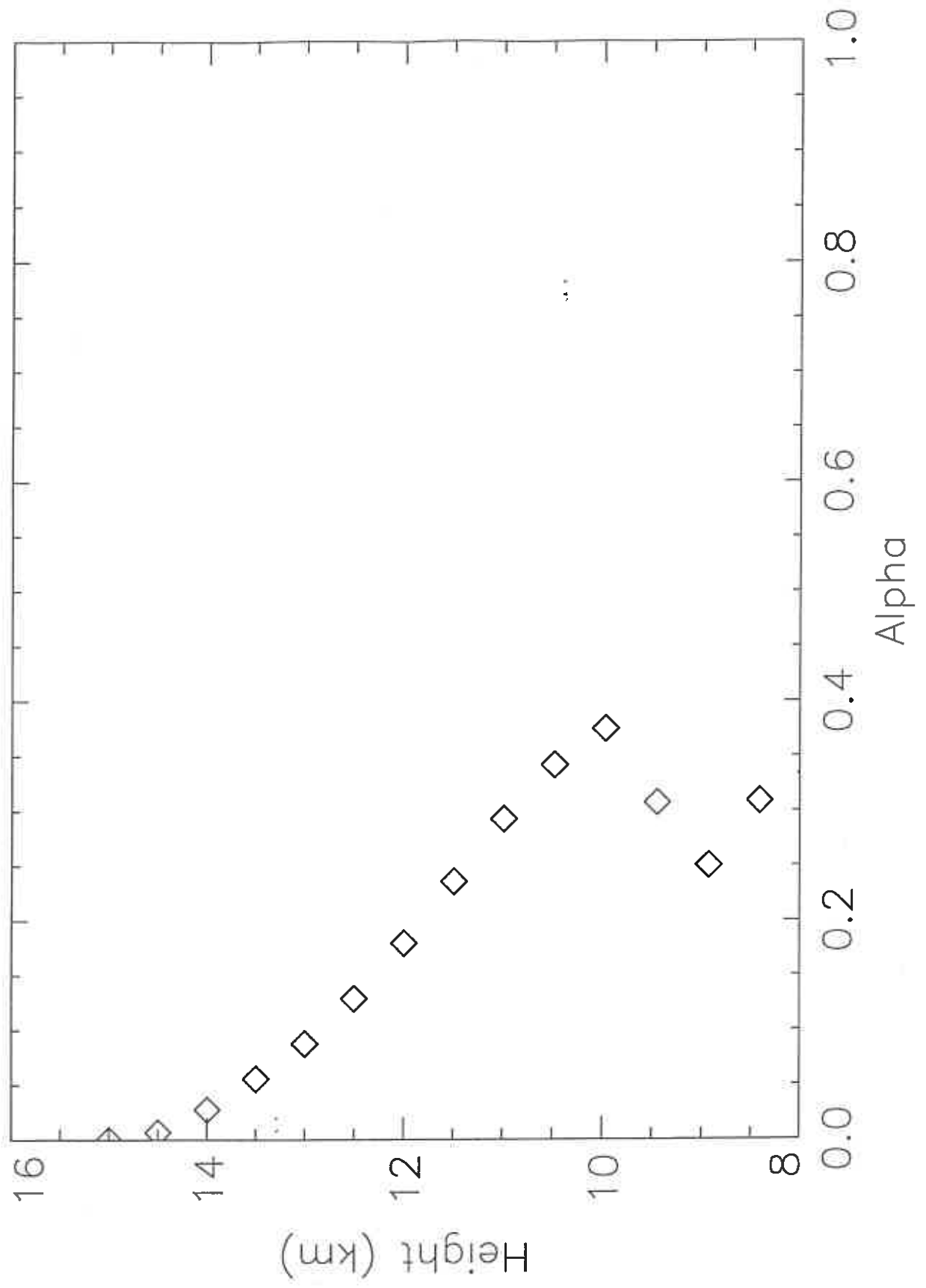


Figure 16: Vertical profile of momentum flux from 2nd hour of [164] (solid), [204] (dashed) and [231] (dash-dotted).

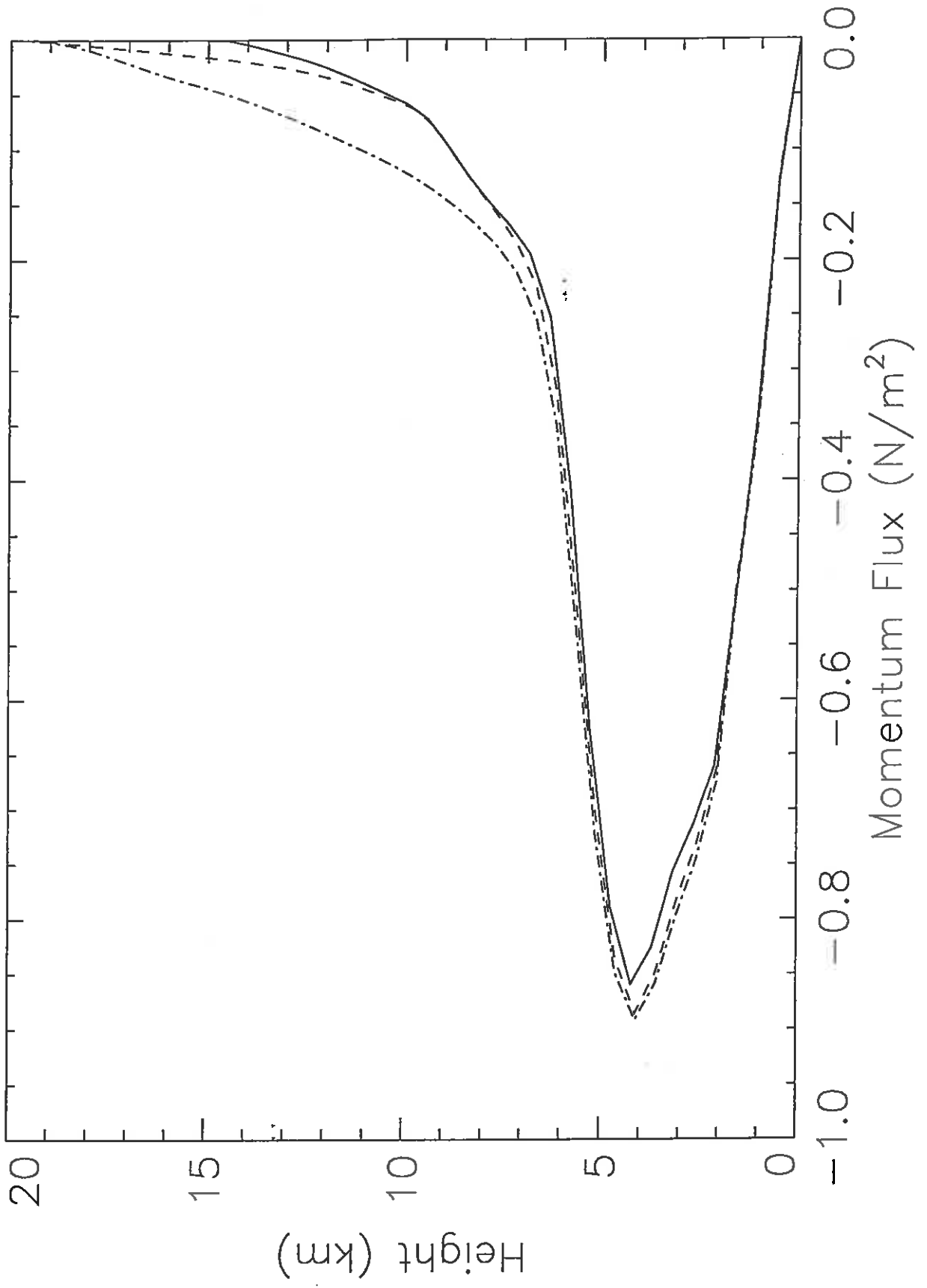


Figure 17: Vertical profile of  $\alpha$  above 8km from second and subsequent hours of [204].

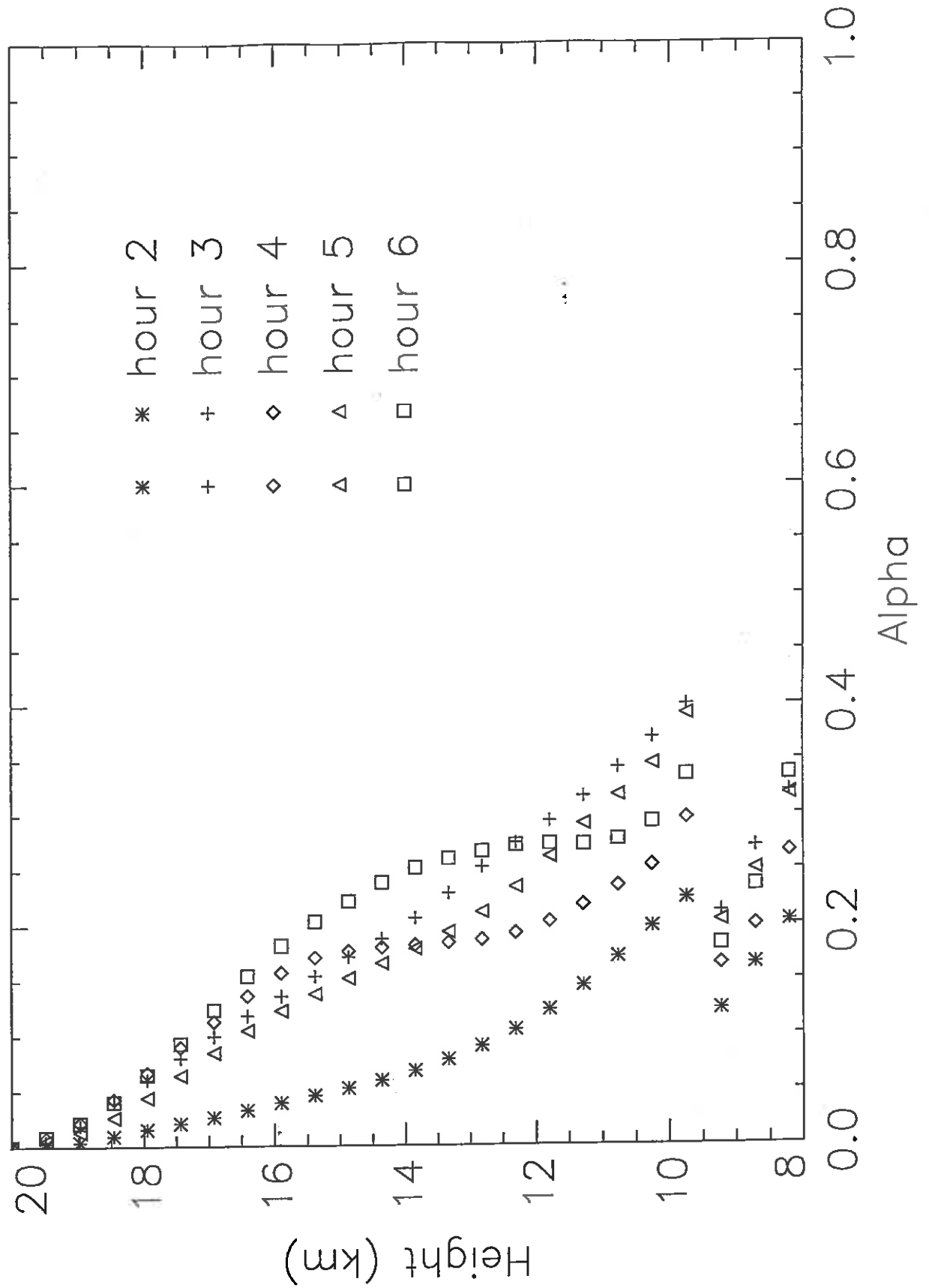


Figure 18: Vertical profile of  $\alpha$  above 8km from second and subsequent hours of [231].

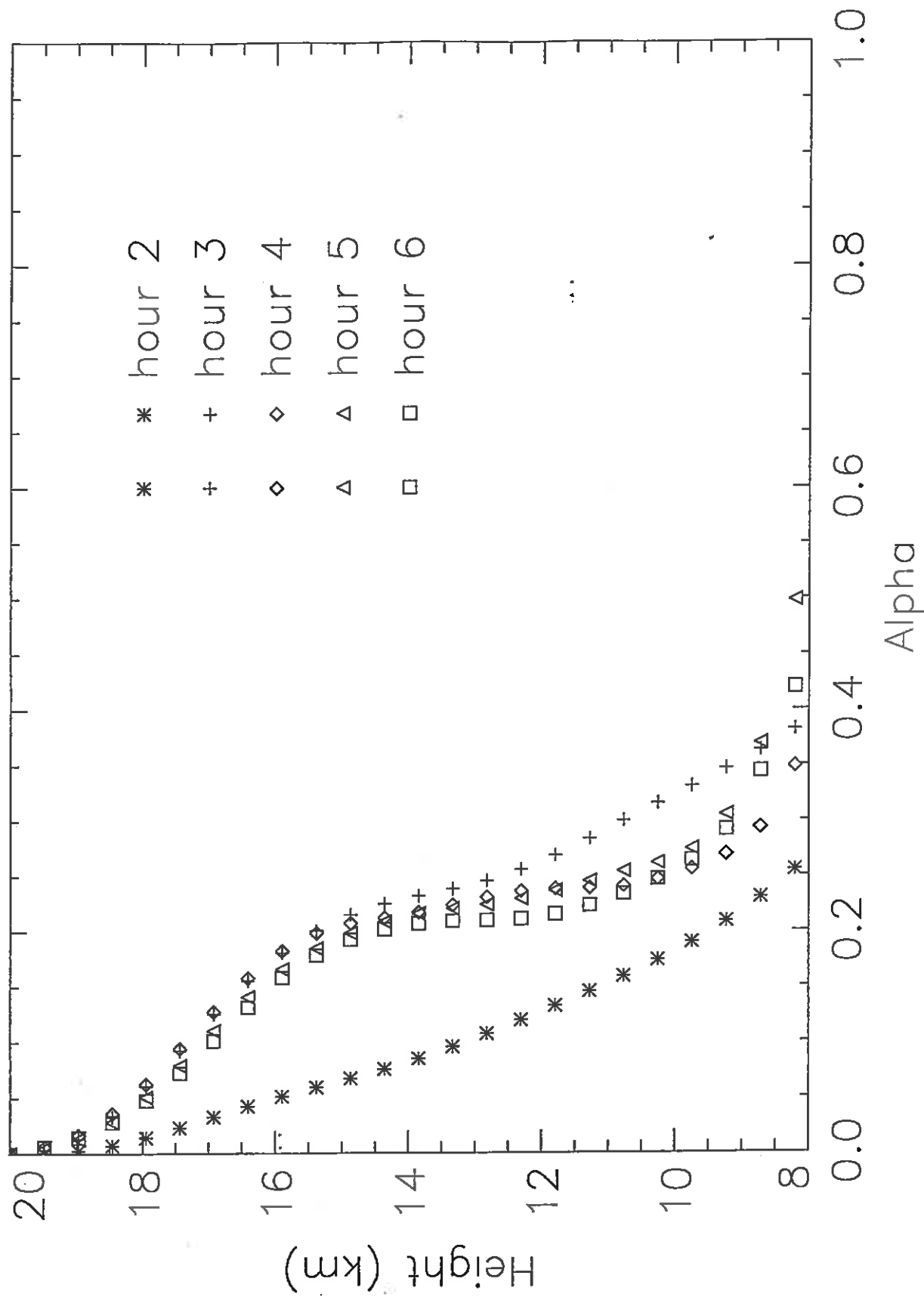
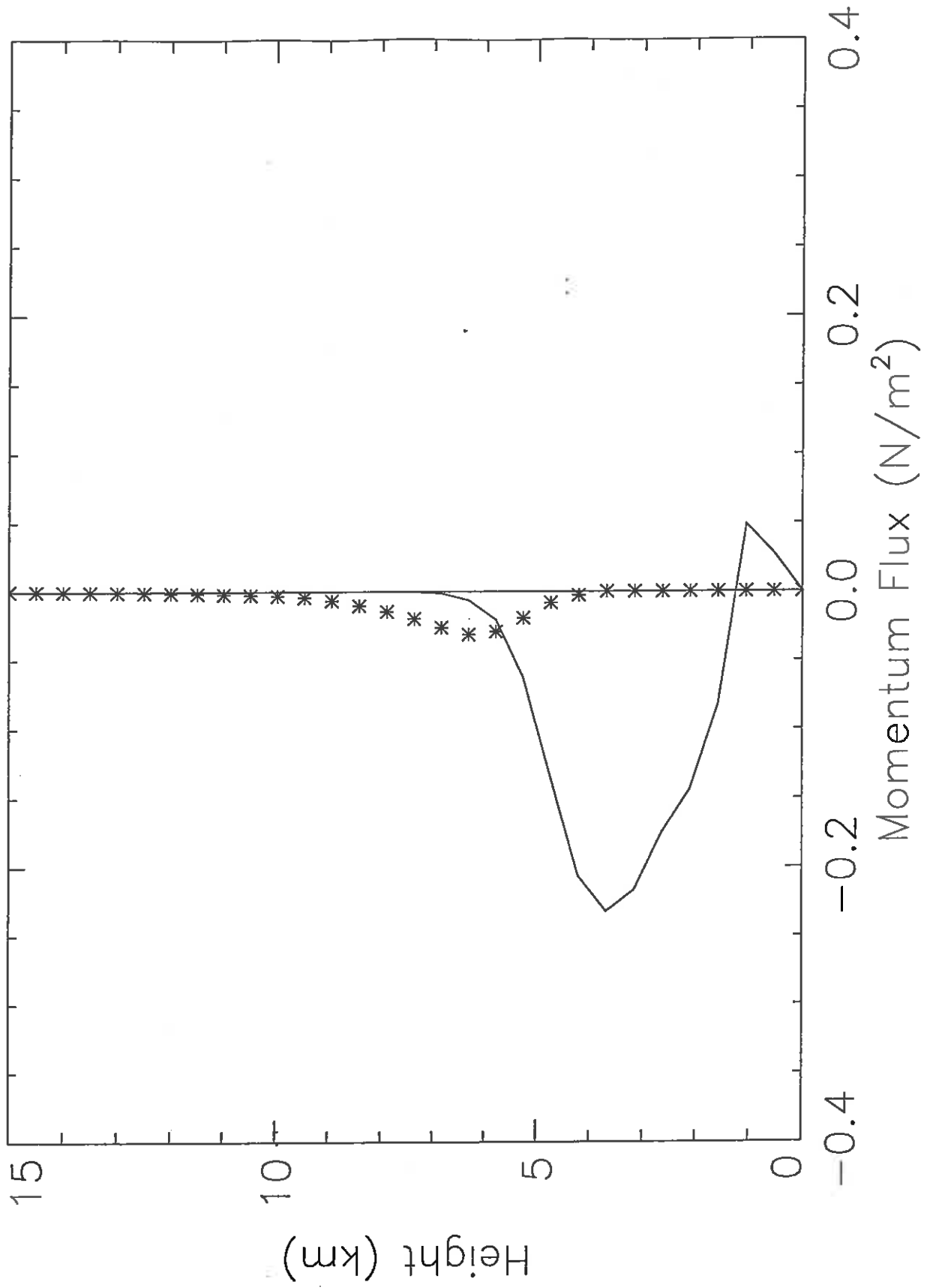


Figure 19: Vertical profile of partitioned momentum fluxes from the 2nd hour of a repeat of the control simulation with additional diagnostics (solid line: convective flux; stars: wave flux).



## CURRENT JCMM INTERNAL REPORTS

This series of JCMM Internal Reports, initiated in 1993, contains unpublished reports and also versions of articles submitted for publication. The complete set of Internal Reports is available from the National Meteorology Library on loan, if required.

1. **Research Strategy and Programme.**  
K A Browning et al  
January 1993
2. **The GEWEX Cloud System Study (GCSS).**  
GEWEX Cloud System Science Team  
January 1993
3. **Evolution of a mesoscale upper tropospheric vorticity maximum and comma cloud from a cloud-free two-dimensional potential vorticity anomaly.**  
K A Browning  
January 1993
4. **The Global Energy and Water Cycle**  
K A Browning  
July 1993
5. **Structure of a midlatitude cyclone before occlusion.**  
K A Browning and N Roberts  
July 1993
6. **Developments in Systems and Tools for Weather Forecasting.**  
K A Browning and G Szejwach  
July 1993
7. **Diagnostic study of a narrow cold frontal rainband and severe winds associated with a stratospheric intrusion.**  
K A Browning and R Reynolds  
August 1993
8. **Survey of perceived priority issues in the parametrizations of cloud-related processes in GCMs.**  
K A Browning  
September 1993
9. **The Effect of Rain on Longwave Radiation.**  
I Dharssi  
September 1993

10. **Cloud Microphysical Processes - A Description of the Parametrization used in the Large Eddy Model.**  
H Swann  
July 1994
11. **An Appreciation of the Meteorological Research of Ernst Kleinschmidt.**  
A J Thorpe  
May 1992
12. **Potential Vorticity of Flow Along the Alps.**  
A J Thorpe, H Volkert and Dietrich Heimann  
August 1992
13. **The Representation of Fronts.**  
A J Thorpe  
January 1993
14. **A Parametrization Scheme for Symmetric Instability: Tests for an Idealised Flow.**  
C S Chan and A J Thorpe  
February 1993
15. **The Fronts 92 Experiment: a Quicklook Atlas.**  
Edited by T D Hewson  
November 1993
16. **Frontal wave stability during moist deformation frontogenesis. Part 1. Linear wave dynamics**  
C H Bishop and A J Thorpe  
May 1993
17. **Frontal wave stability during moist deformation frontogenesis. Part 2. The suppression of non-linear wave development.**  
C H Bishop and A J Thorpe  
May 1993
18. **Gravity waves in sheared ducts.**  
S Monserrat and A J Thorpe  
October 1993
19. **Potential Vorticity and the Electrostatics Analogy: Quasi-Geostrophic Theory.**  
C Bishop and A J Thorpe  
November 1993
20. **Recent Advances in the Measurement of Precipitation by Radar.**  
A J Illingworth  
April 1993

21. **Micro-Physique et Givrage. Cloud Microphysics and Aircraft Icing.**  
A J Illingworth  
May 1993
22. **Differential Phase Measurements of Precipitation.**  
M Blackman and A J Illingworth  
May 1993
23. **Estimation of Effective Radius of Cloud Particles from the Radar Reflectivity.**  
N I Fox and A J Illingworth  
May 1993
24. **A Simple Method of Dopplerising a Pulsed Magnetron Radar.**  
L Hua, A J Illingworth and J Eastment  
November 1993
25. **Radiation and Polar Lows.**  
George C Craig  
February 1994
26. **Collected preprints submitted to International Symposium on the Life Cycles of Extratropical Cyclones; Bergen, Norway, 27 June - 1 July 1994**  
April 1994
27. **Convective Frontogenesis**  
Douglas J Parker and Alan J Thorpe  
April 1994
28. **Improved Measurement Of The Ice Water Content In Cirrus Using A Total Water Evaporator**  
Philip R A Brown and Peter N Francis  
April 1994
29. **Mesoscale Effects of a Dry Intrusion within a Vigorous Cyclone**  
K A Browning and B W Golding  
April 1994
30. **GEWEX Cloud System Study, Science Plan**  
May 1994
31. **Parametrization of Momentum Transport by Convectively Generated Gravity Waves**  
R Kershaw  
February 1995
32. **Mesoscale Modelling Newsletter, No. 5**  
May 1994

33. **Observations of the mesoscale sub-structure in the cold air of a developing frontal cyclone**  
K A Browning, S A Clough, C S A Davitt, N M Roberts and T D Hewson  
May 1994
34. **Longwave Radiative Forcing of a Simulated Tropical Squall Line**  
Imtiaz Dharssi  
July 1994
35. **On the nature of the convective circulations at a kata-cold front**  
K A Browning  
September 1994
36. **Collected preprints of papers submitted to the COST-75 International Seminar on Advanced Weather Radar Systems, Brussels, 20-23 September 1994**  
November 1994
37. **Use of satellite imagery to diagnose events leading to frontal thunderstorms: Parts I and II of a case study**  
K A Browning and N M Roberts  
November 1994
38. **The role of spaceborne millimetre-wave radar in the global monitoring of ice cloud**  
P R A Brown, A J Illingworth, A J Heymsfield, G M McFarquhar, K A Browning and M Gosset  
December 1994
39. **Potential Vorticity Inversion**  
Michal Ziemianski  
October 1994
40. **Theory of mature tropical cyclones; A comparison between Kleinschmidt (1951) and Emanuel (1986)**  
Suzanne L Gray  
December 1994
41. **Dispersion and removal of pollutants during the passage of an atmospheric frontal system**  
N R Gimson  
December 1994
42. **The role of snow sublimation in frontogenesis**  
D J Parker and A J Thorpe  
December 1994
43. **Potential vorticity and the electrostatics Analogy: Ertel-Rossby formulation**  
A J Thorpe and C H Bishop  
December 1994

44. **Mesoscale aspects of extratropical cyclones: an observational perspective**  
K A Browning  
January 1995
  
45. **A Polar Low Outbreak: Evolution and Mesoscale Structures**  
T D Hewson, G C Craig and C Claud  
February 1995

**Met Office** Joint Centre for Mesoscale Meteorology Department of Meteorology  
University of Reading PO Box 243 Reading RG6 6BB United Kingdom  
Tel: +44 (0)118 931 8425 Fax: +44 (0)118 931 8791  
[www.metoffice.com](http://www.metoffice.com)

